Effects of fro and HzO on andesite phase relations between 2 and 4 kbar

Caroline Martel, Michel Pichavant, François Holtz, Bruno Scaillet, Jean-Louis Bourdier, Hervé Traineau

JOURNAL OF GEOPHYSICAL RESEARCH, VOL. 104, NO. B12, PAGES 29,453–29,470, DECEMBER 10, 1999

Effects of f_{O_2} and H_2O on andesite phase relations between 2 and 4 kbar

Caroline Martel,[1] Michel Pichavant, Francois Holtz, and Bruno Scaillet

Centre de Recherches sur la Synthèse et la Chimie des Minéraux, Centre National de la Recherche Scientifique, Orléans France

Jean-Louis Bourdier

Département des Sciences de la Terre and UMR 6530, Université d'Orléans, Orléans, France

Hervé Traineau

Bureau de Recherches Géologiques et Minières, Orléans, France

Abstract. Experimental phase equilibria have been investigated on three medium-K silicic andesite (60-61 wt % SiO_2) samples from Mount Pelée at 2-4 kbar, 850-1040°C, under both vapor-saturated CO_2-free and vapor-saturated CO_2-bearing conditions. Most experiments were crystallization experiments using dry glasses prepared from the natural rocks. Both normal- and rapid quench experiments were performed. Two ranges of oxygen fugacity (f_{O_2}) were investigated: NNO (Ni-NiO buffer) to NNO + 1 and NNO + 2 to NNO + 3. At 2 kbar for moderately oxidizing conditions, plagioclase (pl) and magnetite (mt) are the liquidus phases, followed by low-Ca pyroxene (opx); these three phases coexist over a large temperature (T)-H_2O range (875-950°C and 5-7 wt % H_2O in melt). Amphibole (am) is stable under near vapor-saturated CO_2-free conditions at 876°C. At 900°C, ilmenite (ilm) is found only in experiments less than or equal to NNO. Upon increasing pressure (P) under vapor-saturated CO_2-free conditions, pl + mt is replaced by am + mt on the liquidus above 3.5 kbar. For highly oxidizing conditions, mt is the sole liquidus phase at 2 kbar, followed by pl and opx, except in the most H_2O-rich part of the diagram at 930°C, where opx is replaced by Ca-rich pyroxene (cpx) and am. Compositions of ferromagnesian phases systematically correlate with changing f_{O_2} Experimental glasses range from andesitic through dacitic to rhyolitic, showing systematic compositional variations with pl + opx + mt fractionation (increase of SiO_2 and K_2O, decrease of Al_2O_3, CaO, FeO^t, and MgO). FeO*/MgO moderately increases with increasing SiO_2. For f_{O_2} conditions typical of calk-alkaline magmatism (approximately NNO + 1), magnetite is either a liquidus or a near-liquidus phase in hydrous silicic andesite magmas, and this should stimulate reexamination for the mechanisms of generation of andesites by fractionation from basaltic parents.

1. Introduction

Arc magmatism, volumetrically second to ocean floor magmatism, is the key for understanding the formation of continents and material recycling into the mantle. Andesites form an important fraction of arc igneous rocks, and much effort has been devoted to elucidate their petrogenesis. Andesites have been considered to represent primary magmas, generated by melting of either basalts from the subducting slab [*Green and Ringwood*, 1968; *Kay*, 1978; *Defant and Drummond*, 1990; *Yogodzinski et al.*, 1994] or peridotite from the mantle wedge [e.g., *Kushiro et al.*, 1972; *Nicholls and Ringwood*, 1973; *Mysen et al.*, 1974; *Green*, 1976]. A second group of models interprets andesites and the felsic igneous rocks of the calc-alkaline series as fractionation products of primitive, mantle-derived, basaltic magmas [e.g., *Stern*, 1979; *Gill*, 1981; *Sisson and Grove*, 1993a, b]. Magma mixing [e.g., *Eichelberger, 1975*] and assimilation are also known to play important roles in the genesis of andesites.

A limited number of phase equilibrium studies on andesites have been performed under simultaneously controlled melt H_2O content and f_{O_2} [*Eggler*, 1972; *Eggler and Burnham*, 1973; *Maksimov et al.*, 1978; *Ritchey and Eggler*, 1978; *Sekine et al.* 1979; *Baker and Eggler*, 1987]. The influence of H_2O on liquidus and solidus temperatures of andesitic magmas and on crystallization sequences and the conditions of amphibole stability have been determined up to 10 kbar and above. However, the compositions of coexisting minerals and melts have remained largely unknown, in part because most of these studies were performed before routine use of the electron microprobe and also because of iron loss and quenching

1 Now at Bayerisches Geoinstitut, Universität Bayreuth, Bayreuth, Germany

Paper number 1999JB900191.
0148-0227/99/1999JB900191$09.00

Table 1. Composition of Starting Materials

	1929 Dome (D29)		P1 Fallout (P1R)		P1 Surge (P1D)	
	WR[a]	Glass[b]	WR[a]	Glass[b]	WR[a]	Glass[b]
SiO_2	61.11	62.19	60.75	62.06	60.97	63.17
TiO_2	0.48	0.50	0.43	0.43	0.45	0.46
Al_2O_3	17.74	17.49	17.48	17.63	17.47	17.76
Fe_2O_3	3.10	-	2.11	-	1.97	-
FeO	3.26	6.39[c]	4.04	6.21[c]	4.19	5.47[c]
MnO	0.18	0.14	0.17	0.14	0.18	0.13
MgO	2.29	2.28	2.17	2.27	2.20	1.98
CaO	6.24	6.35	6.16	6.50	6.15	6.27
Na_2O	3.53	3.59	3.45	3.67	3.53	3.67
K_2O	1.05	1.06	0.97	1.08	1.03	1.14
H_2O	0.37	ND	1.68	ND	0.77	ND
Total	99.35	100.00	99.41	100.00	98.91	100.00

[a]Whole-rock analysis (wet chemical technique; FeO by titration).
[b]Average of electron microprobe analyses, recalculated to 100%.
[c]Total Fe as FeO.
ND, not discernible

problems [*Sisson and Grove*, 1993a]. These earlier studies were all carried out under relatively reducing conditions (Fayalite-Magnetite-Quartz $\leq f_{O_2} \leq$ NNO), now known to be inappropriate to the crystallization of typical island arc andesites (f_{O_2} around NNO + 1 [see *Gill*, 1981]). There is clearly a need for additional experiments on andesites under carefully controlled f_{O_2} conditions above NNO.

In addition to being of fundamental petrological interest, andesites commonly erupt from island arc volcanoes, such as at Mount Pelée (Martinique), one of the active volcanoes of the Lesser Antilles island arc. For understanding volcanic processes and better evaluating the potential associated hazards, knowledge of the preeruptive conditions of equilibration of andesitic magma bodies is a prerequisite. Conditions of magma storage, in particular, melt H_2O contents, have a profound influence on eruptive style (e.g., explosive versus effusive). Studies of phase equilibria at low pressures, appropriate for the storage of the magmas in crustal reservoirs, constitute one of the best approaches for the determination of preeruptive conditions, as first demonstrated on the Mount St. Helens dacites [*Rutherford et al.*, 1985; *Rutherford and Devine*, 1988].

In order (1) to provide new experimental data applicable to the petrogenesis of andesites and (2) to determine the preeruptive storage conditions of silicic andesite magmas (SiO_2 ~ 60 wt %) tapped by eruptions of Mount Pelée eruptions, an experimental phase equilibrium study has been performed on three Mount Pelée andesites at pressure (P) $\leq$ 4 kbar. In this paper the effects of f_{O_2} and melt H_2O content on andesite phase relations are detailed, with emphasis placed on the stability of ferromagnesian phases and on compositional variations. The application of the experimental data to the recent Mount Pelée eruptions forms the subject of C. Martel et al. (manuscript in preparation, 1999).

2. Experimental and Analytical Methods

2.1. Experimental Methods

2.1.1. Starting materials and charges. The experiments were performed in parallel on three medium-K silicic andesite samples with nearly identical compositions (Table 1), typical of compositions erupted during the recent period of activity at Mount Pelée [*Fichaut et al.*, 1989; *Smith and Roobol*, 1990]. The selected samples, however, have different textural characteristics. One is a pumice from the 650 years B.P. Plinian fallout (P1 fallout), whereas the other two are lithic juvenile rocks from the P1 basal surge and the 1929-1932 dome, respectively (the latter is subsequently referred to as the 1929 dome). Modal proportions and phase compositions are fully detailed in the companion paper (C. Martel et al., manuscript in preparation, 1999). The three samples have the same phenocryst assemblage (plagioclase, orthopyroxene, magnetite, rare clinopyroxene, trace ilmenite, and resorbed amphibole) and modal proportions (~45 vol % phenocrysts on a vesicle-free basis). There are minor but detectable differences in the phenocryst compositions (C. Martel et al., manuscript in preparation, 1999). Plagioclase rim compositions range from An55 to An60 in the two P1 samples and from An50 to An55 in the 1929 dome sample. In the latter, orthopyroxenes tend to be more Mg-rich than in the P1 samples, the result of near-surface oxidation that is also apparent in the whole rock FeO/Fe_2O_3 data (Table 1).

Most experiments were crystallization experiments starting from glasses. However, during the initial stages of the study, melting experiments were also performed directly using andesite powders ground to <50 μm, run together with the crystallization experiments (Table 2). In spite of the relatively long run durations (typically 1-2 weeks at 850-900°C), we experienced difficulty in distinguishing between the newly formed phases and the residual, inherited crystals. When refractory phases such as plagioclase are involved, bulk equilibrium probably can not be attained in melting experiments of any reasonable durations. Consequently, crystallization experiments were preferred. The experimental strategy followed one established previously for phase equilibrium studies of felsic magmas [e.g., *Pichavant*, 1987; *Holtz et al.*, 1992; *Scaillet et al.*, 1995; *Scaillet and Evans*, 1999]. Dry glasses were used as starting materials. In so doing, during the heating up period, melts are forced to cross a T-H_2O domain of high ΔT and intermediate H_2O contents where crystal nucleation is promoted [e.g., *Fenn*, 1977]. Each rock was ground in an agate mortar to ~50 μm, loaded in a Pt capsule, and then fused twice (with grinding in between) for 4 hours at 1400°C and 1 atm. The glasses obtained were analyzed by electron microprobe and their compositions compared with the whole rock wet chemical data (Table 1). Relative differences (average values of 0.8% (SiO_2), 1% (Al_2O_3, CaO), 2% (Na_2O), 5% (FeO^t, MgO), and 6% (K_2O)) are within analytical errors. The electron microprobe analysis of Fe in both Pt capsules and glasses before and after fusion showed that Fe loss during fusion is negligible. The three glasses were ground to <20 μm.

Charges consisted of the glass powder (~30 mg) plus water (distilled and deionized) and silver oxalate, as source of CO_2. Both CO_2-free and CO_2-bearing experiments were carried out. All experiments were performed in presence of a fluid phase and are vapor-saturated. The vapor phase consists essentially of either pure H_2O (experiments subsequently referred to as vapor-present CO_2-free or more simply by CO_2-free) or H_2O-CO_2 fluid mixtures (experiments subsequently referred to as vapor-present and CO_2-bearing or more simply by CO_2-bearing). Initial fluid compositions ($XH_2Oin.$ = $XH_2O/(XH_2O+XCO_2)$ in moles) were 1 (CO_2-free system), 0.9, 0.8, and 0.7 (H_2O-CO_2 mixtures). The fluid/silicate ratio (mass of fluid components/(mass of fluid components + glass

Table 2. Experimental Conditions and Results

Charge	XH_2Oin.	H_2O in Glass, wt %	a_{H_2O}, bars	$\log f_{O_2}$, bars	ΔNNO	Results[a]	ΣR^2	Fe Loss,[b] %
			Run X1, 2028 bars, 850°C, f_{H_2} = 1.0 bars, 235 hours					
D29/1	0.79	5.5[c]	0.82	- 11.0	+ 1.8	gl(47), pl(40), opx(8), mt(5)	0.43	< 1
			Run X5, 2130 bars, 876°C, f_{H_2} = 3.5 bars, 322 hours					
D29/2	1	6.9	1	- 11.4	+ 0.9	gl(59), pl(27), opx(5), mt(3), am(6)	0.23	< 1
D29/3	0.89	6.5	0.94	- 11.4	+ 0.9	gl(54), pl(33), opx(7), cpx(3), mt(3)	0.07	< 1
D29/4	0.81	6.15	0.88	- 11.5	+ 0.8	gl(44), pl(42), opx(11), mt(3)	0.15	< 1
P1R/1	1	6.9	1	- 11.4	+ 0.9	gl(60), pl(29), opx(7), mt(3), am(1)	0.36	< 1
P1R/2	0.90	6.45	0.94	- 11.4	+ 0.9	gl(53), pl(36), opx(9), mt(2)	0.12	< 1
P1R/3	0.80	6.15	0.89	- 11.5	+ 0.8	gl(45), pl(44), opx(8), cpx(1), mt(2)	0.07	< 1
P1D/1	1	6.9/7.3	1	- 11.4	+ 0.9	gl(57), pl(32), opx(7), cpx(1), mt(3)	0.20	< 1
P1D/2	0.90	6.6	0.96	- 11.4	+ 0.9	gl(54), pl(33), opx(6), cpx(4), mt(3)	0.10	< 1
P1D/3	0.79	6.3	0.93	- 11.4	+ 0.9	gl(46), pl(41), opx(10), mt(3)	0.15	< 1
			Run X2, 2150 bars, 902°C, f_{H_2} = 3.6 bars, 270 hours					
D29/5	0.79	5.5[c]	0.81	- 11.0	+ 0.8	gl(55), pl(33), opx(9), mt(3)	1.03	< 1
P1D/4	0.82	5.5[c]	0.80	- 11.0	+ 0.8	gl(48), pl(40), opx(9), mt(3)	0.38	< 1
			Run X17, 1980 bars, 900°C, f_{H_2} = 5.5[c] bars, 123 hours					
P1D/5[d]	1	6.9	1	- 11.3	+ 0.6	gl(68), pl(23), opx(5), cpx(1), mt(3)	0.04	< 1
P1D/6[d]	0.88	6.1	0.89	- 11.4	+ 0.5	gl(57), pl(32), opx(9), mt(2)	0.21	< 1
			Run X4, 2205 bars, 903°C, f_{H_2} = 5.9 bars, 302 hours					
D29/6	1	6.9	1	- 11.2	+ 0.6	gl(66), pl(22), opx(8), mt(3), am[e]	0.45	< 1
D29/7	0.89	6.2	0.90	- 11.3	+ 0.5	gl(55), pl(33), opx(9), mt(3), am[e]	0.26	< 1
D29/8	0.79	5.6	0.81	- 11.4	+ 0.4	gl(49), pl(38), opx(10), mt(3), am[e]	0.10	< 1
D29/9	0.69	5.5	0.79	- 11.4	+ 0.4	gl(45), pl(42), opx(11), mt(2), am[e]	0.18	< 1
P1R/4	1	6.9	1	- 11.2	+ 0.6	gl(72), pl(21), opx(7), mt(<1), am[e]	0.60	+ 1
P1R/5	0.90	6.3	0.95	- 11.3	+ 0.5	gl(61), pl(29), opx(6), cpx(2), mt(2), am[e]	0.39	< 1
P1R/6	0.77	5.5	0.83	- 11.4	+ 0.4	gl(49), pl(39), opx(10), mt(2), am[e]	0.21	< 1
P1R/7	0.70	5.4	0.78	- 11.4	+ 0.4	gl(46), pl(43), opx(10), mt(1)	0.17	< 1
P1D/8	1	6.9	1	- 11.2	+ 0.6	gl(68), pl(21), opx(7), mt(4)	0.48	< 1
P1D/9	0.90	6.1	0.88[c]	- 11.3	+ 0.5	gl(57), pl(31), opx(9), mt(3), am[e]	0.63	< 1
P1D/10	0.80	5.6	0.81	- 11.4	+ 0.4	gl(46), pl(41), opx(11), mt(2), am[e]	0.23	< 1
P1D/11	0.71	5.5	0.79	- 11.4	+ 0.4	gl(46), pl(42), opx(10), mt(2), am[e]	0.37	- 1
			Run X3, 2112 bars, 902°C, f_{H_2} = 9.8 bars, 327 hours					
D29/10	1	6.9	1	- 11.7	+ 0.1	gl(65), pl(23), opx(9), mt(3), am[e]	0.79	< 1
D29/11	0.88	6.2	0.89	- 11.8	0.0	gl(55), pl(32), opx(11), mt(2), ilm(tr), am[e]	0.28	< 1
D29/12	0.80	5.8	0.84	- 11.9	- 0.1	gl(48), pl(38), opx(12), mt(2), ilm(tr), am[e]	0.08	< 1
D29/13	0.71	5.1	0.74[c]	- 12.0	- 0.2	gl(35), pl(47), opx(17), mt(1), am[e]	0.17	+ 1
P1R/8	1	6.9	1	- 11.7	+ 0.1	gl(70), pl(20), opx(8), cpx(tr), mt(2), am[e]	0.44	- 1
P1R/9	0.91	6.2	0.89	- 11.8	0.0	gl(57), pl(34), opx(9), mt(tr), am[e]	0.17	< 1
P1R/10	0.79	5.8	0.83	- 11.9	- 0.1	gl(48), pl(41), opx(10), mt(tr), ilm(tr)	0.25	< 1
P1R/11	0.70	5.7	0.83	- 11.9	- 0.1	gl(40), pl(48), opx(10), mt(2), ilm(tr)	0.10	< 1
P1D/12	1	6.9	1	- 11.7	+ 0.1	gl(63), pl(26), opx(9), mt(2), am[e]	0.76	- 1
P1D/13	0.90	6.2	0.90	- 11.8	0.0	gl(51), pl(37), opx(10), mt(2), ilm(tr)	0.43	< 1
P1D/14	0.80	5.6	0.80	- 11.9	- 0.1	gl(44), pl(44), opx(11), mt(1), ilm(tr)	0.19	< 1
P1D/15	0.70	5.5	0.79	- 11.9	- 0.1	gl(38), pl(49), opx(12), mt(1)	0.11	< 1
			Run X10, 2265 bars, 930°C, f_{H_2} = 1.0 bars, 216 hours					
P1R/12	1	6.9	1	- 9.2	+ 2.2	gl(87), pl(8), cpx(1), mt(2), am(2)	0.21	< 1
P1R/13	0.89	6.1	0.91	- 9.2	+ 2.1	gl(74), pl(20), opx(3), mt(3), am[e]	0.52	< 1
P1R/14	0.80	5.7	0.85	- 9.3	+ 2.1	gl(67), pl(26), opx(4), mt(3), am[e]	0.40	< 1
P1R/15	0.72	5.3	0.78	- 9.4	+ 2.0	gl(55), pl(37), opx(6), mt(2)	0.27	< 1
			Run X9, 2126 bars, 930°C, f_{H_2} = 3.0 bars, 238 hours					
P1R/16	1	6.9	1	- 10.1	+ 1.2	gl(77), pl(15), opx(6), mt(1), am[e]	1.93	< 1
P1R/17	0.89	6.45	0.90	- 10.2	+ 1.1	gl(74), pl(18), opx(6), mt(2), am[e]	0.76	< 1
P1R/18	0.80	6.0	0.84[c]	- 10.3	+ 1.1	gl(64), pl(29), opx(6), mt(1), am[e]	0.27	< 1
P1R/19	0.72	5.6	0.77	- 10.4	+ 1.0	gl(58), pl(35), opx(6), mt(1), am[e]	0.17	< 1
			Run X6, 2210 bars, 930°C, f_{H_2} = 4.4 bars, 256 hours					
D29/14	1	6.9	1	- 10.4	+ 0.9	gl(67), pl(21), opx(8), mt(4), am[e]	0.84	< 1
D29/15	0.90	6.4	0.92	- 10.5	+ 0.8	gl(64), pl(24), opx(9), mt(3), am[e]	0.62	< 1
D29/16	0.79	6.05	0.87	- 10.6	+ 0.8	gl(55), pl(34), opx(9), mt(2), am[e]	0.30	< 1
D29/17	0.71	5.5	0.78	- 10.7	+ 0.7	gl(51), pl(37), opx(10), mt(2)	0.29	< 1
P1R/20	1	6.9	1	- 10.4	+ 0.9	gl(72), pl(18), opx(7), mt(3), am[e]	0.98	< 1
P1R/21	0.90	6.4	0.92	- 10.5	+ 0.8	gl(68), pl(22), opx(8), mt(2), am[e]	0.41	< 1
P1R/22	0.81	5.8	0.83	- 10.6	+ 0.8	gl(61), pl(29), opx(8), mt(2), am[e]	0.14	< 1
P1R/23	0.70	5.4	0.79	- 10.6	+ 0.7	gl(55), pl(34), opx(9), mt(2), am[e]	0.76	< 1
P1D/16	1	6.9	0.88	- 10.6	+ 0.8	gl(63), pl(25), opx(9), mt(3), am[e]	0.37	< 1
P1D/18	0.79	5.6	0.79	- 10.6	+ 0.7	gl(54), pl(35), opx(9), mt(2), am[e]	0.17	< 1
P1D/19	0.70	5.5	0.77	- 10.7	+ 0.7	gl(48), pl(40), opx(11), mt(2), am[e]	0.30	< 1
			Run X7, 2117 bars, 950°C, f_{H_2} = 0.9 bars, 184 hours					
D29/18	1	6.9	1	- 8.7	+ 2.3	gl(94), pl(1), mt(5), am[e]	3.96	+ 1
D29/19	0.89	6.7	0.96	- 8.8	+ 2.2	gl(75), pl(16), opx(6), mt(3), am[e]	0.21	< 1
D29/20	0.80	6.3	0.90	- 8.8	+ 2.2	gl(66), pl(24), opx(7), mt(3), am[e]	0.63	< 1
D29/21	0.72	6.2	0.88	- 8.9	+ 2.2	gl(60), pl(30), opx(7), mt(3), am[e]	0.12	< 1
P1R/24	1	6.9	1	- 8.7	+ 2.3	gl(95), pl(1), mt(4), am[e]	2.75	< 1
P1R/27	0.71	5.5	0.77	- 9.0	+ 2.0	gl(63), pl(29), opx(6), mt(2), am[e]	0.15	< 1
P1D/20	0.80	6.3[c]	0.91	- 8.8	+ 2.2	gl(62), pl(28), opx(7), mt(3), am[e]	1.03	< 1
P1D/21	0.72	6.0[c]	0.87	- 8.9	+ 2.2	gl(59), pl(31), opx(5), cpx(3), mt(2), am[e]	0.57	< 1

Table 2. (continued)

Charge	$XH_2Oin.$	H_2O in Glass, wt %	a_{H_2O}, bars	$\log f_{O_2}$, bars	ΔNNO	Results[a]	ΣR^2	Fe Loss,[b] %
Run X15, 2126 bars, 951°C, f_{H_2} = 4.3[c] bars, 48 hours								
P1D/22[d]	1	6.9/6.2	1	- 10.1	+ 0.9	gl(95), pl(4), mt(1)	0.15	< 1
P1D/23[d]	0.86	5.9	0.85	- 10.2	+ 0.8	gl(81), pl(14), opx(4), mt(1)	0.04	< 1
P1D/24[d]	0.80	5.8	0.83	- 10.3	+ 0.7	gl(76), pl(18), opx(5), mt(1)	0.03	< 1
P1D/25[d]	0.74	5.5	0.80	- 10.3	+ 0.7	gl(68), pl(25), opx(6), mt(1)	0.05	< 1
Run X8, 2102 bars, 1003°C, f_{H_2} = 0.5 bars, 140 hours								
D29/22	1	6.9	1	- 7.3	+ 2.9	gl(95), mt(5), am[e]	3.75	+ 1
D29/23	0.89	6.7	0.97	- 7.4	+ 2.8	gl(94), pl(2), mt(4), am[e]	3.63	+ 1
D29/24	0.80	6.3	0.93[c]	- 7.4	+ 2.8	gl(83), pl(12), mt(5), am[e]	4.65	+ 1
P1D/26	1	6.9	1	- 7.3	+ 2.9	gl(95), mt(5), am[e]	4.17	+ 1
P1D/27	0.89	6.6[c]	0.95	- 7.4	+ 2.8	gl(93), pl(3), mt(4), am[e]	3.04	+ 1
P1D/28	0.79	6.3[c]	0.93	- 7.4	+ 2.8	gl(83), pl(12), mt(5), am[e]	5.71	+ 1
P1D/29	0.71	5.3[c]	0.77	- 7.6	+ 2.6	gl(61), pl(28), opx(7), mt(4), am[e]	1.00	< 1
Run X12, 2170 bars, 1041°C, f_{H_2} = 0.4 bars, 53 hours								
P1D/30	1	6.9	1	- 6.4	+ 3.2	gl(100), mt(tr), am[e]	0.27	< 1
P1D/31	0.89	5.4	0.78	- 6.7	+ 3.0	gl(99), mt(1), am[e]	0.50	+ 1
P1D/32	0.80	4.0	0.53	- 7.0	+ 2.6	gl(100), mt(tr), am[e]	0.25	+ 1
Run X16, 3125 bars, 925°C, f_{H_2} = 6.8[c] bars, 71 hours								
P1D/33[d]	1	7.6	1	- 10.6	+ 0.8	gl(76), pl(18), opx(6), mt(tr)	0.07	< 1
P1D/34[d]	0.88	5.8	0.77	- 10.8	+ 0.6	gl(55), pl(34), opx(11), mt(tr), ilm(tr)	0.04	< 1
Run X11, 4160 bars, 925°C, f_{H_2} = 9.8 bars, 170 hours								
P1D/35	1	10.8	1	- 10.6	+ 0.8	gl(82), mt(2), am(16), am[e]	1.26	< 1
P1D/36	0.89	10.5	0.97	- 10.6	+ 0.8	gl(69), pl(19), opx(9), mt(3), am[e]	2.01	< 1
P1D/37	0.80	8.9	0.82	- 10.8	+ 0.6	gl(63), pl(26), opx(10), mt(1), am[e]	1.03	< 1
P1D/38	0.72	6.7	0.61	- 11.0	+ 0.4	gl(60), pl(29), opx(11), mt(tr), ilm(tr), am[e]	0.33	< 1

$XH_2Oin.$, initial H_2O / (H_2O + CO_2) in the charge; H_2O in glass by difference (see text); second number by Karl-Fischer titration; a_{H_2O} calculated from H_2O in glass using the model of *Burnham* [1979] (see also text); $\log f_{O_2}$ calculated from experimental f_{H_2} (see text) and calculated f_{H_2O} (obtained from a_{H_2O}); ΔNNO = $\log f_{O_2}$ - $\log f_{O_2}$ of the NNO buffer calculated at P and T [*Chou*, 1987]; gl, glass; pl, plagioclase; opx, low-Ca pyroxene; cpx, high-Ca pyroxene; mt, magnetite; ilm, ilmenite; am, amphibole; tr, trace.

[a] Phase proportions in weight percent are given in parentheses, calculated by mass balance (see text).

[b] Apparent loss or gain of FeO calculated as (FeO_{calc} - $FeO_{starting\ sample}$) / $FeO_{starting\ sample}$.

[c] Estimated from the other experiments (see text).

[d] Rapid-quench experiment.

[e] quench phase.

powder)) was kept constant, around 10 wt %, to avoid significant changes of the silicate composition by incongruent dissolution in the fluid phase [*Holtz et al.*, 1992]. Because of the small fluid/silicate ratios and the initially dry starting glasses, the equilibrium fluid phase composition differs from $XH_2Oin.$, reflecting the markedly different solubilities of H_2O and CO_2 in silicic liquids at low pressures [see *Holtz et al.*, 1992, Figure 1]. For most runs, Au capsules were used as containers (25 mm long, 2.5 mm ID, 2.9 mm OD). Ag70Pd30 capsules were also used, both in the 1040°C run (Table 2) and in duplicate experiments performed to test for Fe loss. The Au capsules were sealed by arc welding and the AgPd capsules were sealed with a small torch. They were checked for leaks by immersion in an oil bath at 120°C and weighed. Runs were performed with up to 12 capsules (four charges with different $XH_2Oin.$ for each of the three starting samples) kept together under the same P-T-hydrogen fugacity (f_{H_2}) conditions and durations (Table 2).

2.1.2. Equipment and run procedure. All experiments were performed in an internally heated pressure vessel (IHPV) working vertically. Ar-H_2 mixtures were used as pressurizing media in all experiments except for the most oxidized (ΔNNO > 2), where pure Ar was used. Total pressure was continuously recorded by a transducer calibrated against a Heise Bourdon tube gauge (uncertainty ±40 bars, including daily fluctuations). For temperatures below 950°C, a double winding Khantal furnace was used, allowing a quasi-isothermal hot spot 8 cm long [*Roux and Lefevre*, 1992]. Above 950°C another furnace setup [*Roux et al.*, 1994] was used. Temperatures were measured by two to four sheathed chromel-alumel thermocouples (depending on the furnace setup) and recorded continuously. Thermal gradients were mostly within 2°C (up to 8°C for the experiment performed at 1040°C). Typical uncertainties on temperature are ±5°C.

Oxygen fugacity is related to hydrogen fugacity and H_2O fugacity (f_{H_2O}) through the H_2O dissociation reaction. In our experiments, f_{H_2} is imposed (at given P and T) and is a function of the proportion of H_2 initially loaded into the vessel [*Eggler*, 1972; *Eggler and Burnham*, 1973; *Scaillet et al.*, 1992, 1995]. For T < 930°C, f_{H_2} was measured directly and continuously by a Shaw-type semipermeable H_2 membrane located in the hot spot of the furnace [*Scaillet et al.*, 1992]. Uncertainties on H_2 pressure measurements are ±0.5 bar, corresponding to uncertainties on $\log f_{O_2}$ of ±0.05-0.15 for the f_{H_2} range in Table 2. For T > 930°C, Ni-Pd-O sensors were used to determine f_{H_2} [*Taylor et al.*, 1992]. From other studies performed in this laboratory [*Scaillet and Evans*, 1999], f_{H_2} measurements with the H_2 membrane and the Ni-Pd-O sensors agree within 2% for f_{H_2} in the 1-5 bar range. For three runs (Table 2), f_{H_2} was not measured but was estimated from the initial H_2 loaded into the vessel and from the f_{H_2} measurements in other experiments at the same P and T.

Experimental durations varied between 2 and 14 days, decreasing generally with increasing temperature (Table 2). Runs were normally stopped by switching off the power, inducing an averaged temperature drop of 100°C/min. Three experiments were performed with a rapid quench device modified after *Roux and Lefevre* [1992]. A thin alumina tube holding the capsules was hung in the furnace hot spot by two Khantal wires (0.2 mm diameter). At the end of the experiment the Khantal wires were fused electrically, allowing the sample

holder to fall instantaneously into the cold part (~50°C) of the vessel (temperature drop of ~100°C/s) under quasi-isobaric conditions. After the experiment each capsule was weighed to check for leaks and then opened. For each charge a clast of run product was embedded in an epoxy resin, polished, then studied by scanning electron microscopy (SEM), and analyzed by electron microprobe.

2.2. Analytical Methods

2.2.1. Major elements. The electron microprobe analyses were performed with either a Cameca Camebax or a Cameca SX 50 (Services Communs BRGM-CNRS-Université, Orléans), under an acceleration voltage of 15 kV and a counting time of 10 s. Silicate minerals were used as standards. Sample currents of either 6 or 12 nA and beam sizes of 1-2 μm were employed for mineral phases and 6 nA and either 10 or 5 μm for glasses. In the latter, the measured alkali concentrations were corrected using secondary standards [e.g., *Pichavant*, 1987], which were three bubble-free hydrous rhyolitic glasses, nearly identical in composition to the experimental glass samples, containing 2.0, 4.6, and 6.3 wt % H_2O. They were synthesized by hydration, at 1300°C, 4 kbar for 3 days of matrix glass fragments separated from a pumice sample of the P1 eruption from Mount Pelée, then analyzed for H_2O by Karl-Fischer titration [*Behrens et al.*, 1996] and for the alkalies by wet chemical techniques. Correction factors varied from 0.95 to 1.2 for Na_2O and from 0.95 to 1.1 for K_2O, depending on the glass H_2O content. For the different oxides analyzed, the analytical errors are 1% (SiO_2, Al_2O_3, CaO), 3% (FeO, MgO, TiO_2), and 5% (MnO, Na_2O, K_2O). Mass balance calculations [*Albarède*, 1995] were performed on all major oxides except MnO and H_2O to estimate the proportions of phases coexisting in a given charge and to evaluate the extent of Fe loss.

2.2.2. H_2O. The H_2O content of the experimental glasses was systematically measured since it could not be estimated from the composition of the fluid phase [e.g., *Eggler and Burnham*, 1973], which is unknown. Because most charges contain a significant proportion of crystals homogeneously distributed in the glass (Table 2), infrared spectroscopy could not be used as a routine method for H_2O analysis. The glass H_2O contents were thus measured using the "by-difference" method [*Devine et al.*, 1995]. The difference from 100% of electron microprobe analyses (after correction of the alkalies) was calibrated against the dissolved glass H_2O content by using the three hydrous glasses described above as standards, analyzed together with the experimental glasses during each microprobe session.

Despite the use of the secondary standard glasses, H_2O contents measured with our by-difference method were anomalously too high (by several weight percent) in a number of glasses (but not all) from the 2 kbar experiments. This problem was not encountered in the rapid quench experiments and is therefore not of analytical nature. In the normal-quench experiments, quenching is not isobaric and glasses could either microvesiculate or hydrate locally (since a fluid phase is always present), while temperature drops, leading in both cases to higher apparent H_2O concentrations. Therefore the anomalously high H_2O contents found in all the 2 kbar normal-quench experiments were corrected against the data for the rapid quench experiments. H_2O contents of glasses from the 900 and 951°C, 2 kbar, CO_2-free rapid quench experiments are identical (6.9 wt %, Table 2) and this value was taken as the H_2O content for all the ~2 kbar CO_2-free experiments (Table 2). Analysis by Karl-Fischer titration of the 951°C, 2 kbar, CO_2-free rapid quench charge and of one 876°C, 2 kbar, CO_2-free charge (Table 2) yielded 6.2 ± 0.2 and 7.3 ± 0.2 wt % H_2O, respectively. For the CO_2-bearing experiments the corrections were performed by using the dependence between XH_2Oin. and glass H_2O content established from the rapid quench experiments. Uncertainties of our glass H_2O content determinations are ±0.5%.

2.2.3. Calculations of f_{O_2}. For each charge the H_2O dissociation reaction was used to compute f_{O_2} from experimental f_{H_2} and calculated f_{H_2O} [*Scaillet et al.*, 1995]. f_{H_2O} was obtained from the H_2O activity (a_{H_2O}), which was calculated from the glass H_2O contents using a thermodynamic model [*Burnham*, 1979]. Because our CO_2-free rapid quench experiments yield analyzed glass H_2O contents slightly higher than the thermodynamic model used (e.g., 6.9 wt % H_2O at 951°C, 2.12 kbar (Table 2) versus 6.0 wt % H_2O for the model), a_{H_2O} values from the model were normalized so as to give unity for glass H_2O contents corresponding to our CO_2-free rapid quench experiments. This procedure maintains the internal consistency of our H_2O concentration data, avoids handling values of $a_{H_2O} > 1$ (Table 2), and affects the f_{O_2} calculations by < 0.1 log unit. Overall uncertainties on individual log f_{O_2} determinations are ±0.25 log units. For a given experiment (constant P-T-f_{H_2}), the average variation of f_{O_2} between charges with different XH_2Oin. (and consequently a_{H_2O}) is 0.3 log unit, the maximum being 0.6 log unit (run X12, Table 2). For comparison, compositions of three pairs of coexisting magnetites and ilmenites in run X3 (2.1 kbar, 902 ± 5°C, Tables 2 and 3) yield ΔNNO/T(°C) values of -0.3/849, -0.6/875, and -0.2/934 using the solid solution model for Fe-Ti oxides of *Ghiorso and Sack* [1991] and -1.2/858, -0.4/809 and -0.1/840 using the model of *Andersen et al.* [1993], whereas experimental ΔNNO values are 0.0, 0.0, and -0.1, respectively (Table 2).

3. Experimental Results

Since the objectives of the study are to provide experimental information on the phase equilibria of silicic andesite magmas under relatively oxidizing conditions and at low pressures, most of the experiments were performed at ~2 kbar, with a few additional ones at 3 and 4 kbar (Table 2). T was varied between 850 and 1040°C to cover most of the crystallization interval of the magmas. Two ranges of f_{O_2} were investigated (Figure 1): NNO to NNO + 1 (subsequently termed "moderately oxidizing" or "low" f_{O_2}) and NNO + 2 to NNO + 3 (subsequently termed "highly oxidizing" or "high" f_{O_2}), so that the effect of varying f_{O_2} above the NNO buffer (calculated at the pressure of interest from *Chou* [1987]) can be determined. Although H_2O contents were varied from CO_2-free to CO_2-bearing conditions, it was not considered relevant to study nearly dry conditions since andesitic magmas from island arcs are known to be distinctly H_2O-rich. At ~2 kbar the investigated melt H_2O contents range from ~4 to ~7 wt % H_2O. Experimental conditions and results are detailed in Table 2.

3.1. Run Products and Attainment of Equilibrium

Run products consisted of fluid, glass, and mineral phases. Plagioclase, low-Ca pyroxene, and magnetite were found systematically in most experiments, whereas Ca-rich pyroxene,

Table 3. Selected Experimental Compositions

Charge	Phase	SiO_2	TiO_2	Al_2O_3	FeO	MnO	MgO	CaO	Na_2O	K_2O	Total	Mole Percent
					Run X1: 2028 bars, 850°C, f_{H2}=1 bar, ΔNNO = +1.8, 235 hours							
D29/1	gl(4)[b]	78.13(32)[c]	0.30(6)	12.21(8)	1.35(15)	0.10(8)	0.41(3)	2.09(12)	2.90(6)	2.52(17)	92.35	
	pl(1)	53.65	0.09	28.78	0.87	0.00	0.05	12.39	4.28	0.19	100.32	An61Or1
	opx(3)	54.23(70)	0.13(5)	1.72(29)	16.95(27)	1.58(8)	24.14(10)	1.43(13)	0.04(3)	0.05(4)	100.24	En68Wo3
	mt(1)	1.56	3.96	2.35	83.28	0.69	1.84	0.37	0.12	0.00	94.18	Mt89
					Run X5, 2130 bars, 876°C, f_{H2}=3.5 bars, ΔNNO = +0.8/+0.9, 322 hours							
D29/2	gl(4)	72.66(72)	0.32(6)	15.03(27)	2.36(41)	0.20(8)	0.32(12)	3.57(22)	3.60(21)	1.93(5)	89.60	
	pl(2)	52.54(77)	0.02(0)	28.95(17)	0.96(13)	0.04(4)	0.19(12)	13.08(18)	3.40(12)	0.23(2)	99.43	An67Or1
	opx(2)	53.22(10)	0.16(5)	1.53(30)	20.78(2)	1.07(9)	21.93(35)	1.66(34)	0.09(3)	0.04(0)	100.48	En62Wo3
	mt(2)	0.24(5)	7.03(13)	2.92(5)	81.72(1)	0.51(3)	1.57(13)	0.11(2)	0.01(1)	0.02(0)	94.12	Mt79
	am(6)	47.08(91)	1.31(14)	9.24(30)	13.90(72)	0.45(5)	13.22(49)	10.13(25)	1.75(16)	0.22(6)	97.31	
P1D/1	gl(2)	71.45(36)	0.42(8)	14.81(1)	3.46(8)	0.09(9)	0.64(21)	3.81(3)	3.76(5)	1.56(3)	90.64	
	pl(2)	54.48(46)	0.03(1)	27.87(56)	0.90(10)	0.13(3)	0.07(1)	12.35(25)	3.53(3)	0.19(5)	99.56	An65Or1
	opx(4)	52.60(25)	0.20(3)	1.71(13)	20.66(62)	1.04(10)	21.58(27)	1.87(22)	0.03(1)	0.01(1)	99.68	En61Wo4
	cpx(4)	51.11(6)	0.43(11)	3.00(40)	11.67(30)	0.74(8)	13.63(27)	18.99(48)	0.35(10)	0.03(1)	99.69	En40Wo40
	mt(3)	0.17(1)	7.64(8)	2.89(9)	81.61(14)	0.58(3)	1.62(3)	0.11(2)	0.00(0)	0.02(2)	94.64	Mt78
D29/3	gl(4)	73.31(12)	0.36(6)	14.08(11)	2.68(10)	0.17(8)	0.58(6)	3.11(14)	3.53(9)	2.18(9)	90.62	
	pl(1)	52.38	0.02	28.34	1.05	0.00	0.12	11.52	4.32	2.18	97.95	An59Or1
	opx(4)	51.77(22)	0.19(4)	1.64(7)	22.66(25)	0.97(8)	20.39(32)	1.60(15)	0.03(3)	0.00(0)	99.26	En59Wo3
	cpx(1)	51.2	0.41	2.49	13.67	0.87	13.37	17.25	0.44	0.05	99.76	En39Wo36
	mt(2)	0.28(12)	9.06(23)	2.72(3)	78.41(49)	0.61(10)	1.29(7)	0.20(5)	0.03(3)	0.00(0)	92.61	Mt73
P1R/2	gl(4)	73.67(49)	0.32(4)	14.47(30)	2.41(13)	0.04(4)	0.28(6)	2.93(13)	3.57(24)	2.30(6)	89.97	
	pl(1)	54.05	0.08	27.25	1.34	0.04	0.08	11.72	4.39	0.29	99.25	An57Or2
	opx(3)	52.42(36)	0.21(2)	1.80(29)	23.10(48)	0.84(9)	20.55(9)	1.81(33)	0.05(2)	0.01(1)	100.79	En58Wo4
	mt(1)	0.25	8.48	2.77	77.31	0.34	1.29	0.08	0.07	0.02	90.59	Mt74
D29/4	gl(1)	74.41	0.36	13.32	2.55	0.13	0.34	2.39	4.09	2.42	92.31	
	pl(2)	55.63(92)	0.12(6)	26.72(93)	1.11(21)	0.05(5)	0.11(0)	10.89(66)	4.55(12)	0.24(2)	99.43	An56Or1
	opx(2)	51.66(11)	0.23(3)	1.15(1)	24.82(40)	1.26(15)	18.96(29)	2.17(11)	0.05(5)	0.01(1)	100.31	En54Wo4
	mt(1)	0.22	10.39	2.36	76.25	0.57	1.44	0.14	0.00	0.04	91.41	Mt69
					Run X2, 2150 bars, 902°C, f_{H2} = 3.60 bars, ΔNNO = +0.8, 270 hours							
P1D/4	gl(4)	73.06(21)	0.36(4)	14.22(13)	3.30(26)	0.12(7)	0.55(7)	2.99(12)	3.26(9)	2.14(11)	92.28	
	pl(2)	55.24(34)	0.04(4)	26.70(18)	0.69(13)	0.02(2)	0.11(2)	11.08(35)	4.38(6)	0.26(6)	98.53	An60Or1
	opx(1	51.83(77)	0.16(8)	1.5(88)	23.92(54)	0.98(20)	19.44(51)	1.15(22)	0.02(3)	0.01(1)	99.03	En59Wo3
	mt(2)	1.90(4)	8.96(19)	4.18(5)	72.68(16)	0.58(4)	1.67(11)	0.20(14)	0.17(3)	0.07(2)	90.42	Mt71
					Run X17, 1980 bars, 900°C, f_{H2} = 3.80 bars, ΔNNO = +0.5/+0.6, 123 hours							
P1D/5[d]	gl(2)	69.69(8)	0.37(1)	15.19(3)	3.74(1)	0.18(4)	1.07(0)	4.29(5)	4.05(0)	1.42(2)	91.97	
	pl(3)	50.71(27)	0.02(1)	30.00(13)	1.08(24)	0.04(3)	0.06(2)	13.69(27)	3.37(6)	0.06(2)	99.02	An69Or0
	opx(3)	52.03(38)	0.18(4)	2.05(37)	20.36(44)	0.92(12)	22.52(31)	1.43(19)	0.14(10)	0.02(3)	99.65	En63Wo3
	cpx(2)	51.03(18)	0.38(1)	2.56(31)	11.87(36)	0.63(19)	13.73(41)	18.98(88)	0.25(1)	0.01(1)	99.44	En40Wo40
	mt(5)	0.31(8)	6.66(14)	3.08(8)	80.14(58)	0.52(11)	1.74(6)	0.17(3)	0.01(2)	0.01(2)	92.65	Mt80
P1D/6[d]	gl(7)	71.57(35)	0.37(4)	14.52(30)	3.53(20)	0.13(8)	0.79(4)	3.51(24)	3.81(7)	1.76(4)	92.40	
	pl(1)	53.27	0.00	28.98	0.87	0.08	0.02	12.16	4.40	0.16	99.95	An60Or1
	opx(6)	51.42(26)	0.19(3)	1.65(29)	21.83(69)	1.19(13)	20.46(43)	1.82(23)	0.04(2)	0.02(4)	98.61	En59Wo4
	mt(2)	0.51(9)	7.98(8)	2.73(1)	80.53(42)	0.34(19)	1.47(4)	0.22(3)	0.06(6)	0.02(2)	93.87	Mt76
					Run X4, 2205 bars, 903°C, f_{H2} = 5.85 bars, ΔNNO = +0.4/+0.6, 302 hours							
D29/6	gl(4)	71.75(54)	0.45(4)	15.14(65)	3.02(50)	0.16(4)	0.24(8)	4.21(8)	3.50(16)	1.53(5)	92.40	
	pl(1)	48.3	0.00	31.38	0.68	0.00	0.07	14.81	2.81	0.06	98.11	An74Or0
	opx(2)	52.28(9)	0.16(1)	2.57(35)	18.83(37)	0.96(1)	22.87(79)	1.74(15)	0.06(3)	0.01(0)	99.48	En65Wo4
	mt(1)	0.33	7.46	4.05	79.16	0.35	1.89	0.17	0.00	0.00	93.42	Mt77
P1R/5	gl(2)	72.23(6)	0.43(1)	15.01(9)	2.79(12)	0.16(2)	0.35(5)	3.57(5)	3.27(5)	2.21(6)	89.51	
	pl(1)	52.42	0.07	28.70	1.76	0.00	0.08	12.33	3.77	0.16	99.30	An64Or1
	opx(2)	52.30(32)	0.17(2)	1.93(4)	19.48(21)	0.96(7)	22.32(24)	1.66(14)	0.04(4)	0.01(1)	98.87	En64Wo3
	cpx(1)	52.41	0.36	2.15	14.00	0.68	15.84	14.05	0.17	0.04	99.69	En46Wo29
	mt(2)	0.36(13)	9.74(3)	3.16(1)	76.24(3)	0.37	1.48	0.36	0.04(3)	0.04(3)	91.80	Mt70
D29/7	gl(1)	71.71	0.53	14.94	3.06	0.24	0.21	3.55	3.64	2.11	90.64	
	pl(2)	54.66(43)	0.08(8)	27.66(55)	1.21(13)	0.02(2)	0.10(4)	11.70(17)	3.84(1)	0.25(2)	99.52	An62Or2
	opx(2)	52.42(33)	0.18(1)	2.15(12)	19.15(75)	0.98(3)	21.94(16)	2.36(86)	0.08(2)	0.01(1)	99.29	En63Wo5
	mt(2)	0.89(14)	10.12(9)	3.16(1)	75.77(40)	0.39(0)	1.49(1)	0.25(4)	0.07(3)	0.04(2)	92.19	Mt69
D29/9	gl(4)	73.59(49)	0.51(3)	13.55(12)	3.30(30)	0.06(5)	0.40(8)	2.68(14)	3.46(2)	2.46(2)	92.33	
	pl(1)	56.25	0.09	27.19	1.00	0.00	0.10	10.93	4.51	0.26	100.34	An56Or2
	opx(4)	50.97(15)	0.22(2)	1.30(21)	26.49(11)	0.91(7)	17.28(35)	1.70(26)	0.02(1)	0.01(1)	98.89	En51Wo4
	mt(2)	0.29(3)	14.09(73)	2.58(3)	73.88(66)	0.52(3)	1.50(9)	0.14(5)	0.06(4)	0.02(1)	92.73	Mt57
P1D/11	gl(2)	72.95(53)	0.45(10)	13.61(9)	3.34(48)	0.27(0)	0.48(2)	2.85(8)	3.54(11)	2.51(13)	93.10	
	pl(2)	55.71(29)	0.07(3)	26.93(28)	0.83(5)	0.03(1)	0.10(1)	10.80(13)	4.25(17)	0.33(4)	99.05	An57Or2
	opx(1)	50.77	0.20	1.15	25.67	1.01	19.54	1.45	0.09	0.00	99.90	En55Wo3
	mt(1)	0.27	14.21	2.74	74.49	0.40	1.52	0.15	0.03	0.00	93.82	Mt57

Table 3. (continued)

Charge	Phase	SiO_2	TiO_2	Al_2O_3	FeO	MnO	MgO	CaO	Na_2O	K_2O	Total	Mole Percent
Run X3, 2112 bars, 902°C, f_{H2} = 9.75 bars, ΔNNO = -0.2/+0.1, 327 hours												
P1R/8	gl(2)	70.57(25)	0.56(5)	16.12(43)	3.03(16)	0.21(13)	0.23(5)	4.30(18)	3.47(1)	1.50(2)	87.98	
	pl(1)	50.20	0.03	30.74	0.62	0.00	0.04	14.83	3.04	0.08	99.58	An73Or0
	opx(2)	50.96(29)	0.19(3)	1.86(41)	23.26(74)	0.75(2)	21.72(21)	1.68(10)	0.06(2)	0.03(2)	100.51	En60Wo3
	cpx(2)	50.44(23)	0.51(10)	2.52(75)	13.78(22)	0.51(5)	12.94(51)	17.79(10)	0.20(3)	0.01(1)	98.70	En38Wo38
	mt(2)	0.44(25)	12.00(17)	3.24(4)	72.96(70)	0.52(9)	1.68(11)	0.20(4)	0.05(5)	0.01(1)	91.11	Mt63
D29/11	gl(1)	72.04	0.41	14.46	3.97	0.00	0.49	3.22	3.26	2.15	89.81	
	pl(1)	53.23	0.04	28.72	0.75	0.02	0.04	12.64	4.15	0.16	99.76	An62Or1
	opx(1)	51.00	0.22	1.92	25.50	0.80	18.28	1.8	0.09	0.03	99.65	En53Wo4
	mt(3)	0.28(5)	12.71(13)	3.26(5)	73.05(43)	0.55(6)	1.73(2)	0.24(7)	0.00(1)	0.01(1)	91.83	Mt61
	ilm(2)	0.30(7)	47.02(13)	0.21(3)	46.03(20)	0.63(15)	2.58(24)	0.20(3)	0.05(1)	0.01(1)	97.03	Ilm89
P1R/10[e]	gl(4)	73.37(31)	0.45(5)	13.92(10)	3.32(34)	0.06(5)	0.34(5)	2.75(5)	3.26(19)	2.53(6)	91.01	
	pl(4)	54.76(27)	0.07(6)	26.74(30)	1.42(44)	0.01(1)	0.10(0)	10.56(21)	4.48(18)	0.31(5)	98.46	An55Or2
	mt(3)	0.26(4)	14.24(40)	2.86(3)	69.52(11)	0.52(1)	1.56(19)	0.21(1)	0.05(4)	0.03(2)	89.25	Mt55
	ilm(1)	0.08	46.51	0.28	46.00	0.62	2.95	0.18	0.07	0.00	96.69	Ilm87
P1D/15[e]	gl(1)	74.92	0.32	13.34	2.70	0.21	0.25	2.47	3.36	2.43	93.86	
	pl(1)	55.95	0.08	25.37	1.39	0.06	0.51	10.16	4.55	0.28	98.36	An54Or2
	opx(2)	51.13(24)	0.23(1)	1.08(28)	28.88(9)	0.88(2)	15.12(4)	2.08(0)	0.12(6)	0.03(0)	99.57	En45Wo5
Run X10, 2265 bars, 930°C, f_{H2} = 1.00 bar, ΔNNO = +2.0/+2.2, 216 hours												
P1R/12[f]	pl(2)	48.16(42)	0.01(1)	32.43(16)	0.75(9)	0.00(0)	0.04(4)	17.02(35)	1.98(11)	0.08(5)	100.48	An82Or0
	cpx(3)	51.9(74)	0.32(14)	2.52(74)	7.75(19)	0.59(13)	16.06(75)	20.74(73)	0.19(3)	0.02(1)	100.10	En45Wo42
	mt(2)	0.56(35)	2.62(13)	4.11(12)	80.80(64)	0.41(4)	3.41(4)	0.15(7)	0.05(5)	0.00(0)	92.14	Mt93
	am(3)	46.24(31)	1.27(7)	10.03(7)	10.10(5)	0.32(15)	16.30(14)	11.72(25)	1.78(11)	0.19(2)	97.97	
P1R/13	gl(3)	69.46(4)	0.43(4)	15.92(8)	3.72(19)	0.22(10)	1.19(11)	4.53(4)	3.18(14)	1.32(10)	90.92	
	pl(2)	51.91(58)	0.01(1)	29.73(1)	0.95(11)	0.00(0)	0.11(3)	13.67(1)	3.21(9)	0.09(5)	99.67	An70Or1
	opx(2)	54.27(10)	0.14(9)	2.54(11)	12.82(15)	0.87(1)	27.36(23)	1.53(7)	0.08(3)	0.03(3)	99.64	En76Wo3
	mt(3)	0.18(3)	3.58(8)	3.45(5)	82.02(1.0	0.67(6)	2.74(8)	0.15(6)	0.02(1)	0.03(2)	92.83	Mt90
P1R/15	gl(1)	72.62	0.39	13.94	3.67	0.15	0.83	3.25	2.98	2.16	92.36	
	pl(2)	55.34(88)	0.07(1)	26.75(75)	1.67(21)	0.06(0)	0.16(1)	11.01(41)	4.25(11)	0.27(4)	99.58	An58Or2
	opx(1)	53.4	0.07	1.70	15.72	0.95	25.21	1.66	0.06	0.02	98.78	En70Wo3
	mt(3)	0.51(15)	5.02(12)	94(11)	82.33(40)	0.60(6)	2.07(12)	0.18(7)	0.02(3)	0.02(1)	93.69	Mt86
Run X9, 2126 bars, 930°C, f_{H2} = 3.00 bars, ΔNNO = +1.0/+1.2, 238 hours												
P1R/19	gl(4)	70.15(52)	0.55(6)	14.75(22)	4.50(39)	0.15(11)	0.87(17)	3.97(26)	3.10(12)	1.95(20)	92.76	
	pl(2)	56.00(6)	0.09(5)	26.08(9)	1.96(35)	0.05(2)	0.23(0)	10.79(1)	4.19(5)	0.29(1)	99.68	An58Or2
	opx(2)	52.62(4)	0.16(0)	1.24(10)	21.38(39)	0.96(4)	21.05(34)	1.62(0)	0.04(2)	0.03(1)	99.11	En61Wo3
	mt(3)	0.37(11)	8.30(11)	3.17(13)	79.22(47)	0.46(4)	1.74(2)	0.11(6)	0.17(6)	0.01(1)	93.58	Mt75
Run X6, 2210 bars, 930°C, f_{H2}= 4.40 bars, ΔNNO = +0.7/+0.9, 256 hours												
P1D/18	gl(3)	70.23(29)	0.51(4)	14.48(8)	4.84(28)	0.25(9)	0.78(6)	3.69(16)	3.28(24)	1.95(7)	93.85	
	pl(1)	55.46	0.00	27.17	0.98	0.06	0.24	11.25	4.67	0.25	100.09	An56Or1
	opx(2)	51.77(61)	0.26(7)	1.86(33)	24.37(85)	0.93(11)	19.84(11)	1.78(17)	0.02(2)	0.04(1)	100.88	En56Wo4
	mt(3)	0.35(18)	9.67(31)	3.13(14)	77.98(87)	0.59(9)	1.73(3)	0.19(11)	0.04(5)	0.01(1)	93.68	Mt71
Run X7, 2117 bars, 950°C, f_{H2} = 0.90 bar, ΔNNO = +2.0/+2.3, 184 hours												
P1R/24[f]	pl(2)	46.42(26)	0.00(0)	32.60(9)	0.66(16)	0.04(4)	0.05(0)	17.04(17)	1.74(11)	0.03(2)	98.58	An84Or0
	mt(3)	0.18(7)	2.63(5)	5.83(1.4)	81.30(1.0	0.39(23)	3.02(10)	0.15(4)	0.03(5)	0.04(3)	92.45	Mt92
D29/19[f]	pl(4)	51.04(15)	0.02(2)	29.75(27)	1.00(5)	0.01(1)	0.10(1)	13.65(31)	3.53(19)	0.10(2)	99.21	An68Or1
	opx(3)	52.18(33)	0.16(3)	2.54(26)	16.74(21)	0.71(2)	24.88(53)	1.55(19)	0.03(0)	0.01(1)	98.82	En70Wo3
	mt(3)	0.35(6)	3.48(11)	4.26(4)	79.99(81)	0.40(3)	2.88(4)	0.18(6)	0.03(3)	0.02(1)	91.59	Mt90
P1D/21[f]	pl(2)	54.37(24)	0.07(7)	27.42(58)	1.04(5)	0.10(7)	0.10(0)	11.71(11)	4.38(4)	0.17(1)	99.35	An59Or1
	opx(2)	52.56(27)	0.21(4)	1.95(28)	19.71(16)	0.90(13)	22.94(42)	1.52(6)	0.02(2)	0.00(0)	99.82	En64Wo3
	cpx(1)	49.19	0.83	6.16	18.26	0.96	13.39	10.83	0.44	0.10	100.15	En33Wo24
	mt(2)	0.39(3	5.21(8)	13.54(11)	81.23(36)	0.59(12)	2.13(6)	0.21(2)	0.00(0)	0.02(1)	93.32	Mt85
Run X15, 2126 bars, 951°C, f_{H2} = 4.30 bars, ΔNNO = +0.7/+0.9, 48 hours												
P1D/22[d,e]	gl(5)	63.43(22)	0.48(9)	17.17(16)	6.03(38)	0.23(5)	2.21(10)	5.85(10)	3.57(13)	1.04(7)	91.82	
	pl(3)	47.34(31)	0.04(3)	32.25(20)	1.02(5)	0.00(0)	0.08(3)	16.27(12)	2.08(9)	0.06(1)	99.14	An81Or0
P1D/23[d]	gl(3)	65.20(35)	0.53(2)	16.18(5)	6.03(36)	0.12(10)	1.64(3)	5.27(2)	3.74(8)	1.29(6)	92.98	
	pl(1)	49.54	0.00	30.66	0.84	0.11	0.11	14.33	3.25	0.11	98.94	An70Or1
	opx(1)	51.75	0.25	1.99	20.80	0.88	22.73	1.55	0.04	0.03	100.03	En63Wo3
	mt(4)	0.28(16)	8.94(12)	4.24(18)	76.03(48)	0.35(14)	2.05(6)	0.18(10)	0.03(3)	0.03(3)	92.14	Mt72
P1D/24[d,e]	gl(1)	66.07	0.49	15.68	5.93	0.27	1.52	4.94	3.78	1.31	93.09	
	pl(1)	50.56	0.03	29.93	1.22	0.06	0.11	13.93	3.52	0.05	99.41	An68Or0
	opx(2)	52.11(13)	0.27(1)	1.72(23)	21.31(22)	0.73(8)	21.83(2)	1.57(19)	0.01(1)	0.02(2)	99.58	En62Wo3
P1D/25[d,e]	gl(4)	66.82(37)	0.61(1)	15.41(16)	5.88(20)	0.24(9)	1.32(6)	4.68(21)	3.64(13)	1.41(3)	93.38	
	opx(5)	50.72(31)	0.23(9)	1.89(84)	22.78(70)	0.77(13)	20.15(70)	1.84(42)	0.05(7)	0.03(3)	98.46	En58Wo4
Run X8, 2102 bars, 1003°C, f_{H2} = 0.50 bar, ΔNNO = +2.6/+2.9, 140 hours												
P1D/26[f]	mt(2)	0.14(1)	1.26(3)	4.60(6)	84.38(88)	0.39(4)	3.61(3)	0.17(0)	0.00(0)	0.04(2)	94.60	Mt97
P1D/28[f]	pl(1)	47.6	0.00	32.51	1.05	0.00	0.10	16.47	2.05	0.02	99.81	An82Or0
	mt(1)	0.09	1.76	5.08	83.89	0.36	3.56	0.14	0.07	0.05	95.00	Mt95
P1D/29[f]	pl(1)	52.10	0.05	29.1	1.58	0.00	0.18	13.30	3.61	0.16	100.08	An66Or1
	opx(1)	53.49(41)	0.14(0)	2.65(29)	15.29(55)	0.76(6)	26.96(11)	1.13(0)	0.01(0)	0.03(3)	100.47	En73Wo2
	mt(2)	0.24(2)	2.57(7)	4.62(5)	82.85(25)	0.28(4)	3.49(0)	0.15(11)	0.05(1)	0.06(2)	94.31	Mt93

Table 3. (continued)

Charge	Phase	SiO_2	TiO_2	Al_2O_3	FeO	MnO	MgO	CaO	Na_2O	K_2O	Total	Mole Percent
Run X12, 2170 bars, 1041°C, f_{H2} = 0.40 bar, ΔNNO = +2.6/+3.2, 53 hours												
P1D/32	gl(3)	62.34(34)	0.47(4)	17.20(4)	6.50(5)	0.12(9)	2.21(19)	6.45(11)	3.77(8)	0.98(4)	92.75	
	mt(2)	0.24(1)	1.15(0)	5.80(1)	77.74(81)	0.35(2)	3.50(12)	0.16(2)	0.05(5)	0.02(2)	89.03	Mt97
Run X16, 3125 bars, 925°C, f_{H2} = 6.80 bars, ΔNNO = +0.6/+0.8, 71 hours												
P1D/33[d]	gl(7)	66.31(27)	0.53(6)	16.00(13)	5.65(14)	0.16(8)	1.26(4)	4.99(14)	3.76(13)	1.33(7)	91.78	
	pl(2)	50.85(49)	0.03(3)	30.04(20)	0.76(4)	0.06(6)	0.07(1)	14.05(2)	3.36(32)	0.12(0)	99.35	An69Or1
	opx(6)	51.29(81)	0.20(4)	2.35(56)	23.03(46)	0.79(11)	19.34(46)	1.97(24)	0.13(12)	0.02(2)	99.12	En57Wo4
	mt(5)	0.52(25)	10.65(26)	3.71(7)	75.67(80)	0.49(9)	1.68(5)	0.21(8)	0.09(7)	0.05(2)	93.15	Mt67
P1D/34[d,e]	gl(8)	69.89(29)	0.56(2)	14.60(14)	4.74(22)	0.13(6)	0.84(6)	3.91(9)	3.61(4)	1.70(11)	93.07	
	pl(1)	53.90	0.09	27.50	0.91	0.04	0.11	11.36	4.45	0.23	98.60	An58Or1
	opx(8)	51.57(65)	0.21(4)	1.55(45)	26.47(40)	1.02(10)	16.34(46)	2.97(21)	0.18(9)	0.04(5)	100.32	En48Wo6
	mt(1)	1.41	14.09	3.21	71.87	0.47	1.47	0.36	0.09	0.06	93.03	Mt56
Run X11, 4160 bars, 925°C, f_{H2} = 9.8 bars, ΔNNO = +0.4/+0.8, 170 hours												
P1D/35[e,f]	am(6)	42.60(52)	1.01(30)	12.46(48)	17.94(79)	0.41(11)	11.17(41)	9.01(53)	1.66(12)	0.26(7)	96.49	
P1D/37[e,f]	pl(2)	53.08(64)	0.04(4)	28.64(41)	0.96(5)	0.00(0)	0.10(2)	12.78(32)	4.15(4)	0.13(0)	99.88	An63Or1
	opx(2)	50.87(82)	0.22(4)	2.89(19)	24.55(72)	0.78(11)	18.86(0)	1.82(9)	0.06(6)	0.03(3)	100.09	En55Wo4

Abbreviations as in Table 2; Number in parentheses in the second column gives the number of analyses; Numbers in parentheses in the oxide columns are the standard deviation*100.

[a] Glass analyses normalized to 100% anhydrous, with all Fe as FeO. Unnormalized total is reported.

[b] Number of microprobe analyses.

[c] One standard deviation in terms of least unit cited.

[d] Rapid-quench experiment.

[e] Phase assemblage uncompletely analyzed.

[f] Glass composition not given (quench modifications).

ilmenite, and amphibole were less frequently encountered. Apatite was found in some CO_2-free charges below 900°C. The experimental phase assemblages and calculated mass proportions are listed in Table 2.

Plagioclase is of relatively small size (~5-10 μm). It is euhedral, mostly tabular, less frequently with an equant shape. Low-Ca pyroxene is the largest crystalline phase present, with lengths sometimes reaching ~100 μm. It is euhedral and often contains melt inclusions. In some cases, low-Ca pyroxene is rimmed by a quench phase (<2 μm), either amphibole or clinopyroxene, as observed in previous studies [*Eggler*, 1972]. Ca-rich pyroxene is difficult to distinguish optically from either low-Ca pyroxene or amphibole. It is usually smaller in size than low-Ca pyroxene and also lacks the distinctive poikilitic texture. Magnetite, present in all experiments, is characterized by an euhedral, equant habit and a small size (5 μm on average), which makes its analysis by electron microprobe difficult. Ilmenite is very rare and coexists with magnetite in a few experiments (Table 2). Amphibole is present as a stable phase in only a few charges. In these run products, amphibole appears as euhedral stubby prisms 10-15 μm in size.

Most experiments (except the rapid quench) contain quench phases, mainly amphibole (Table 2), yet never occur in greater abundance than a few weight percent. We initially had considerable difficulty in distinguishing between quench and stable amphiboles [*Helz*, 1973, 1976]. However, the rapid quench experiments proved decisive in establishing undoubtly the morphological criteria for identification. Quench amphiboles appear generally as hollow needles whose sizes vary with experimental conditions (~5-10 μm long at 2 kbar, coarser at 4 kbar). Needles of a K-bearing phase, possibly quench biotite, were identified by SEM in the charge P1R/12 (Table 2).

Because the experiments in this study are mostly crystallization experiments starting from glass, equilibrium can not be rigorously demonstrated. However, crystallization experiments are less prone to equilibration problems than melting experiments, as discussed above [e.g., *Green*, 1976; *Pichavant*, 1987; *Holtz et al.*, 1992; *Sisson and Grove*, 1993a; *Scaillet et al.*, 1995; *Scaillet and Evans*, 1999]. The main advantage of crystallization experiments is that most mineral phases grow under the imposed conditions, therefore enabling bulk crystal/liquid equilibrium to be approached, provided that there are no nucleation difficulties. In the early stages of this study we checked that crystallization experiments yielded the same phase assemblage as melting experiments starting from partially crystalline rock powders. Other indications suggesting the absence of nucleation problems in our experiments include textural and morphological criteria (homogeneous crystal distributions, euhedral shapes, plagioclase habits consistent with growth at low ΔT). Mineral phases crystallized in this study are homogeneous, and their compositions vary regularly and smoothly with the experimental conditions (see below and C. Martel et al., manuscript in preparation, 1999). Calculated crystal-liquid exchange coefficient (Kd) are in good agreement with accepted values (see below), suggesting that chemical equilibrium was closely approached.

The presence of quench phases can be taken as another indication that crystals readily nucleated and grew in our experiments. This, however, necessitates an examination of the effect of quench crystallization on the composition of experimental glasses. In all but the rapid quench experiments, glass major element compositions are affected by quench crystallization, but the magnitude of the effects depends on the T-H_2O conditions. Quench crystallization is severe in the high-temperature ($T \geq 930$°C), H_2O-rich charges, where glasses are enriched in SiO_2 and depleted in Na_2O, FeO^t, and MgO (MgO is especially affected because it is often present in concentrations <1 wt % in the experimental glasses). Mass balance calculations for H_2O-rich charges above 930°C commonly have residuals >1 (Table 2). Charges having glass

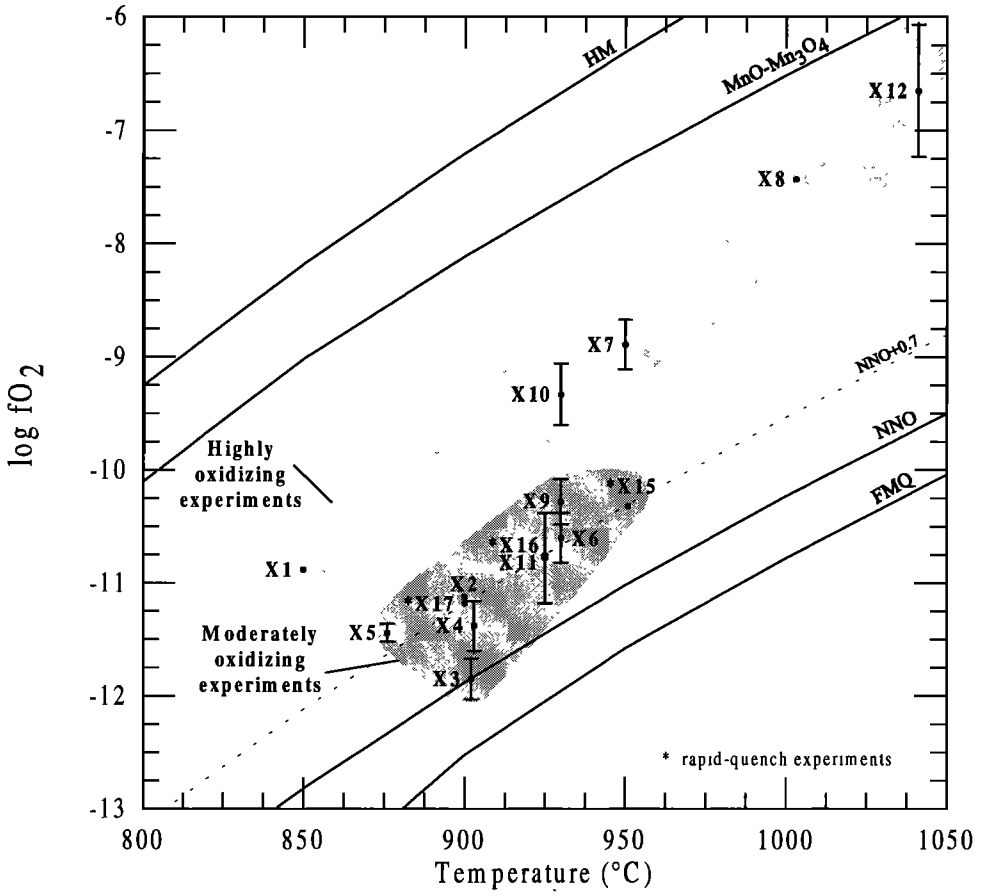

Figure 1. T-f_{O_2} conditions of the Mount Pelée experiments. Oxygen buffer curves calculated for 2 kbar total pressure. Range of f_{O_2} for a given run indicated by error bars. See Table 2 for details.

compositions severely modified because of quench crystallization are specified in Table 3, and the corresponding glass analyses are not considered further.

Calculated mass proportions of run products show that, on average, plagioclase is the most abundant crystalline phase present, followed by low-Ca pyroxene and magnetite. Clinopyroxene, amphibole, and ilmenite rarely exceed 1-3 wt % (see charges D29/2, P1D/2, and P1D/35 in Table 2 for exceptions). For a given run, proportions of glass monotonously decrease with decreasing H_2O content of the melt (melt H_2O). Under comparable T-H_2O melt conditions, increasing pressure causes the proportions of glass to decrease. The proportions of low-Ca pyroxene and magnetite decrease and increase as f_{O_2} increases from NNO/NNO + 1 to NNO + 2/NNO + 3, respectively (Table 2).

Capsules have Fe concentrations below detection (about 500 ppm under our analytical conditions). The Fe content of near-liquidus experimental glasses (P1D/32, Table 3) are identical within error to the starting composition (Table 1). In addition, the mass balance calculations (Table 2) always yield a loss/gain of Fe < 1% relative. This shows that Fe loss to the capsules was not significant in this study.

3.2. Phase Relations

The phase relations are represented in T-H_2O melt diagrams (Figure 2) constructed from the experimental data in Table 2. These diagrams can be considered as isobaric and isooxibaric, despite small pressure and f_{O_2} variations between experiments. Initially, phase diagrams were constructed separately for each of the three samples investigated. However, the experimental results do not change significantly from one starting sample to another, and the resulting diagrams were almost identical. Therefore the phase diagrams presented here combine the experimental data obtained on the three starting samples. In most cases, mineral saturation curves are drawn directly from experimental results. Others are estimated from proportions of mineral phases and their variations with experimental conditions. No attempt was made to locate solidus curves.

The phase relations for moderately oxidizing f_{O_2} (NNO to NNO + 1) at ~2 kbar are shown on Figure 2a. Plagioclase and magnetite are the liquidus phases, followed by low-Ca pyroxene, these three phases crystallizing together within 20-30°C of the liquidus. The relative order of crystallization between magnetite and plagioclase is unknown, since data above 950°C are lacking for this f_{O_2} range. However, judging from their respective mass proportions, the plagioclase saturation curve is probably at a slightly higher temperature than the magnetite (Figures 2a and 3a). Plagioclase, low-Ca pyroxene, magnetite, and liquid coexist over a large T-H_2O range (875-950°C and 5-7 wt % H_2O in melt). Amphibole is stable under near CO_2-free conditions at 876°C (D29/2 and P1R/1, Table 2). Ca-rich pyroxene is present in H_2O-rich charges ≤ 900°C (D29/3, P1R/3, P1R/5, P1R/8, P1D/1, P1D/2, and P1D/5, Table 2). Because Ca-rich pyroxene occurs

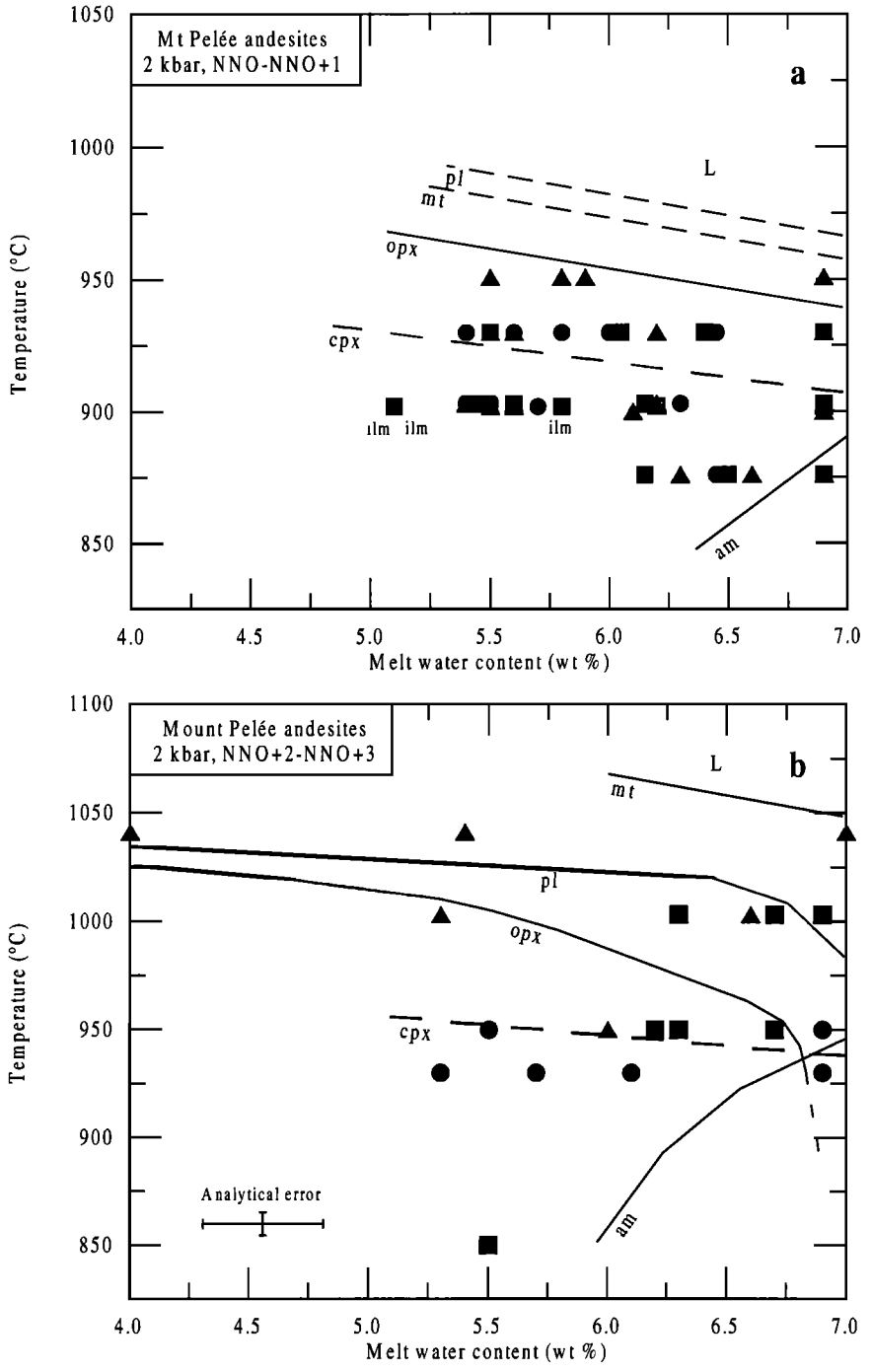

Figure 2. *T*-H_2O melt sections showing the experimentally determined phase equilibria for Mount Pelée andesites at 2 kbar for (a) moderately oxidizing conditions and (b) highly oxidizing conditions. Experiments on different samples indicated by squares, D29; circles, P1R; triangles, P1D (see Table 1). Saturation curves indicated as dashed lines when estimated. L, melt; pl, plagioclase; opx, low-Ca pyroxene; cpx, high-Ca pyroxene; mt, magnetite; ilm, ilmenite; am, amphibole. No saturation curve is drawn for ilmenite because charges less than or equal to NNO are only available for 902°C (see Table 2).

sporadically and in low amounts in run products, the saturation curve drawn for it is approximate. At 2 kbar, ilmenite was found only in the most reduced experiments (run X3, ΔNNO ~ 0, Table 2). No saturation curve is drawn on Figure 2a for ilmenite because experiments with less than or equal to NNO are available for 902°C only.

The phase relations for strongly oxidizing conditions (NNO + 2 to NNO + 3) at ~2 kbar are shown on Figure 2b. The diagram differs from Figure 2a in several aspects. Magnetite crystallizes as the liquidus phase at $T > 1041$°C, followed by plagioclase and low-Ca pyroxene, except in the most H_2O-rich part of Figure 2b, where low-Ca pyroxene is replaced by Ca-rich pyroxene and amphibole (930°C CO_2-free charge P1R/12, Table 2). Ca-rich pyroxene is also present in a CO_2-bearing charge at 950°C (P1D/21, Table 2). Amphibole is stable at 930°C under CO_2-free conditions.

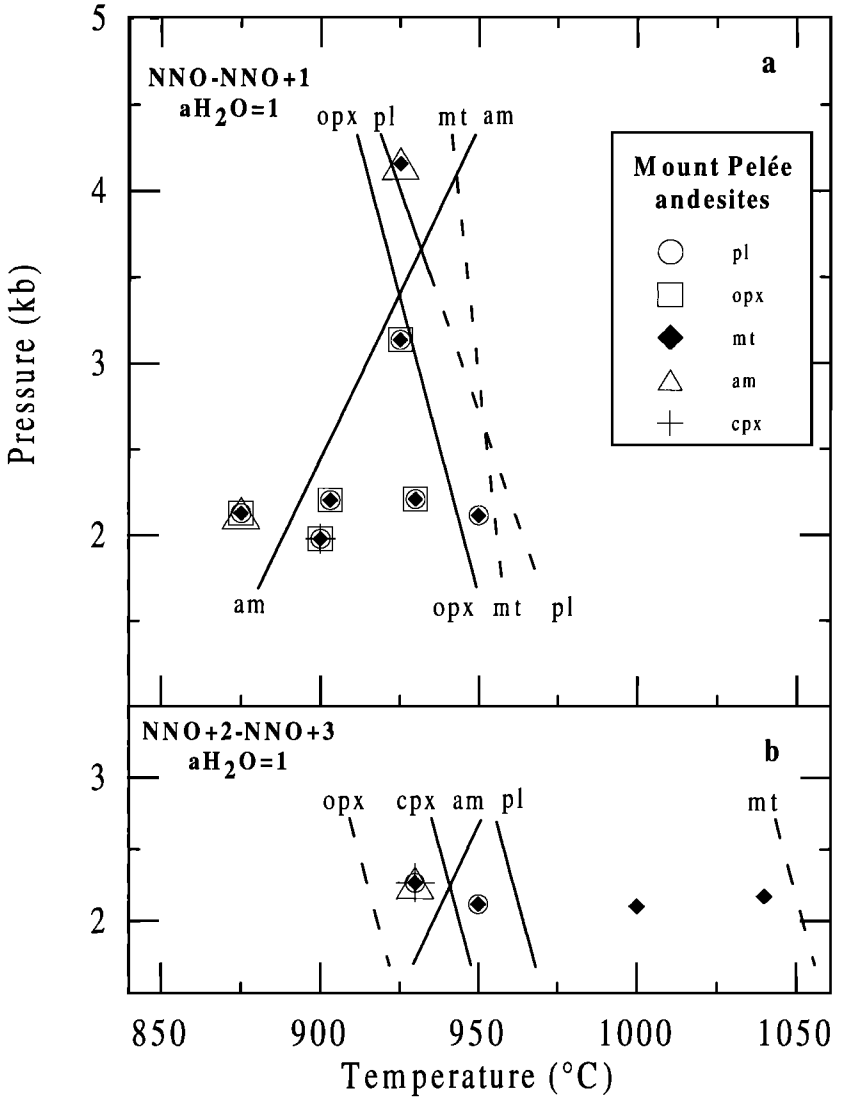

Figure 3. Phase relations for Mount Pelée andesites under CO_2-free conditions: (a) moderately oxidizing conditions and (b) highly oxidizing conditions. Saturation curves are indicated as dashed lines when estimated. pl, plagioclase; opx, low-Ca pyroxene; cpx, high-Ca pyroxene; mt, magnetite; ilm, ilmenite; am, amphibole.

In Figure 2, mineral saturation curves show the expected slopes in T-H_2O melt space, i.e., negative for the anhydrous phases and positive for amphibole [*Eggler and Burnham*, 1973; *Merzbacher and Eggler*, 1984; *Rutherford et al.*, 1985; *Rutherford and Devine*, 1988]. It is stressed that amphibole crystallization is restricted to CO_2-free conditions both at 2 kbar for the two f_{O_2} ranges investigated and at higher pressures for moderately oxidizing conditions (P1D/35, Table 2). Note also that amphibole is absent from the CO_2-bearing 850°C experiment (D29/1, Table 2 and Figure 2b). Therefore the amphibole saturation curves must be relatively steep (i.e., with elevated dT/dH_2O melt).

The CO_2-free phase relations are represented as functions of pressure and temperature on Figure 3 for both series of f_{O_2}. Thus melt H_2O contents progressively increase with increasing pressure on Figure 3. Melt H_2O contents are 7.6 wt % at 3.1 kbar and 10.8 wt % at 4.2 kbar (Table 2). Increasing pressure does not change the stable phase assemblage. Ilmenite was found in the 3.1 kbar, 925°C CO_2-free charge (P1D/34, Table 2) and also in one CO_2-bearing charge at 4.2 kbar, 925°C (P1D/38, Table 2). However, liquidus assemblages vary with pressure. Under moderately oxidizing f_{O_2} (Figure 3a) the relative order of crystallization between plagioclase and low-Ca pyroxene remains unchanged with increasing pressure (Figure 3a). Saturation curves for plagioclase, low-Ca pyroxene, and magnetite all have negative slopes in P-T space, whereas the slope of the amphibole saturation curve is positive, in agreement with previous experimental studies [*Eggler*, 1972; *Eggler and Burnham*, 1973; *Rutherford et al.*, 1985]. Consequently, amphibole + magnetite replaces plagioclase + magnetite on the liquidus above 3.5 kbar. Under strongly oxidizing f_{O_2}, data at pressures higher than 2 kbar are lacking. However, given the wide temperature interval separating the crystallization of magnetite from other phases (Figure 3b), amphibole is not expected to join magnetite on the CO_2-free liquidus before pressures >> 3.5 kbar.

The effect of f_{O_2} on phase equilibria can be illustrated by comparing Figures 3a and 3b. Increasing f_{O_2} from NNO/NNO + 1 to NNO + 2/NNO + 3 leads to: (1) an important decrease in the saturation temperature of low-Ca pyroxene under CO_2-free conditions (~40°C if extrapolated to CO_2-free conditions), concomittant with the appearance of Ca-rich pyroxene and

amphibole, and (2) an important expansion of the amphibole stability field toward higher temperatures (~60°C at 2 kbar). In contrast, the plagioclase saturation temperature is little affected. The magnetite stability field is shown markedly enlarged towards higher temperatures on Figure 3b, although magnetite saturation temperatures at both f_{O_2} are defined only on the basis of their proportions in the different charges.

3.3. Phase Compositions

Phase compositions are given on Table 3. The data have been selected to cover all the investigated P-T-f_{H_2} conditions and the different phase assemblages encountered. However, since the experimental data do not depend on the starting sample, compositions from any of the three samples are given.

Experimental plagioclases have compositions ranging An54-84Ab15-45Or0-2 (±2%) and average FeO^t concentrations between 0.5 and 1.0 wt % (Table 3). They show systematic variations with the experimental parameters. All other parameters being equal, increasing temperature or H_2O content raises An in plagioclase coexisting with low-Ca pyroxene, magnetite, and melt. In contrast, increasing pressure causes a decrease of the plagioclase An content (C. Martel et al., manuscript in preparation, 1999). Plagioclase composition shows no dependence on f_{O_2}. The 2 kbar CO_2-free exchange Kd Ca-Na for plagioclase, defined as (Ca/Na)pl / (Ca/Na)liq, is 3.8 at 900°C and 4.8 at 950°C (calculated from the rapid quench charges P1D/5 and P1D/22, Table 3), in good agreement with values for high-alumina basalts [*Sisson and Grove*, 1993a] under comparable P_{H_2O}-T conditions (4 at 925°C, 5.1 at 950°C, respectively).

Low-Ca pyroxenes have compositions of En45-76Fs18-53Wo2-6 (±2%). Their Al_2O_3 content is <3 wt %, with average values between 1.5 and 2 wt % (Table 3). The En contents of low-Ca pyroxenes in equilibrium with plagioclase, magnetite, and melt systematically vary with melt H_2O content, f_{O_2}, T, and P (Figure 4) (see also C. Martel et al., manuscript in preparation, 1999). All other parameters being equal, increasing temperature, melt H_2O, or f_{O_2} causes En in low-Ca pyroxene to increase, whereas increasing P has the opposite effect. Low-Ca pyroxene-liquid Fe-Mg exchange Kd ranges from 0.27 to 0.26 under CO_2-free conditions at 2 and 3 kbar (charges P1D/5 and P1D/33, Table 3, calculated with total Fe as Fe^{2+}), in good agreement with other experimental data [*Grove et al.*, 1997].

Ca-rich pyroxenes are augites with compositions of En38-46Wo29-42Fs13-25 (Table 3). In only one charge (P1D/21), augite has a subcalcic composition (En33Wo24Fs43, Table 3). Augites have 0.17-0.44 wt % Na_2O, 2.15-3.0 wt % Al_2O_3, and 0.32-0.51 wt % TiO_2, reaching 6.16 wt % Al_2O_3 and 0.83 wt % TiO_2 in the subcalcic augite (Table 3). At equilibrium with plagioclase, orthopyroxene, magnetite, melt ± amphibole, the Wo content of Ca-rich pyroxenes decreases with decreasing melt H_2O content, in agreement with other studies [*Gaetani et al.*, 1993]. Ca-rich pyroxenes become less Fs-rich with increasing f_{O_2}, the smallest Fs (and the highest Wo content, i.e., En45Wo42Fs13, Table 3) being for the 930°C, highly oxidizing, CO_2-free charge P1R/12. The Fe-Mg exchange Kd between Ca-rich pyroxene and liquid is 0.25 at 2 kbar CO_2-free (P1D/5, Table 3, calculated with total Fe as Fe_{2+}) close to 0.23 as determined by *Sisson and Grove* [1993a].

Magnetites are titanomagnetites with TiO_2 up to ~14 wt % in the less oxidizing experiments (Table 3). Using the projection scheme of *Andersen et al.* [1993], magnetites range between Mt55-98Usp2-45 (±2%). They have significant Al_2O_3 and MgO concentrations and detectable MnO (Table 3), similar to those from calc-alkaline volcanic and plutonic rocks [*Gill*, 1981]. Magnetite composition is very sensitive to variations in both f_{O_2} and melt H_2O content and less so to variations in temperature. Compositions of magnetite in the moderately and highly oxidizing experiments are markedly different, i.e., less Ti-rich and more magnesian with increasing f_{O_2} (Figure 5). Ilmenites contain MgO, MnO and Al_2O_3 in decreasing order of abundance; they range between Ilm87-89Hem11-13 (Table 3). Coexisting magnetites and ilmenites in run X3 (Tables 2 and 3) satisfy the equilibrium Mg/Mn partitioning criterion of *Bacon and Hirschmann* [1988].

Experimental amphiboles are hornblendes with 0.3-0.7 cations per formula unit (pfu) in the A site and 1.0-1.7 Al pfu in tetrahedral site (Table 3). Their compositions divide into three groups, each corresponding to the different experimental conditions of amphibole stablility (Figure 6). Amphiboles from the P1D/35 experiment (4.2 kbar, 925°C) have the highest Al^{IV} and number of cations in the A site. At ~2 kbar, amphiboles with lower Al^{IV} for a given number of cations in the A site are obtained. Decreasing temperature from 930 to 876°C strongly reduces the number of cations in the A site and, to a lesser extent, Al^{IV}. Amphibole Fe/(Fe+Mg), calculated assuming all Fe as Fe^{2+}, is strongly dependent on f_{O_2}. Amphiboles from the high f_{O_2} experiment P1R/12 (930°C, 2.3 kbar) have Fe/(Fe+Mg) of ~0.25, markedly lower than for all the other amphiboles crystallized either at the same pressure under less oxidizing conditions (0.35-0.40) or at 4.2 kbar (0.45-0.55, Figure 6).

Glasses have compositions ranging from andesitic through dacitic to rhyolitic (Figure 7), depending on experimental conditions. They show systematic compositional variations with progressive crystallization (i.e., with either decreasing melt H_2O content or temperature, or with increasing pressure, all the other parameters being equal): SiO_2 and K_2O increase while Al_2O_3, CaO, FeO^t, and MgO decrease. Na_2O shows little variation. FeO*/MgO increases with increasing SiO_2 (Figure 7). However, the rate of increase of FeO*/MgO, as defined by the rapid quench experiments, is moderate. The data points straddle the reference boundary between calk-alkaline and tholeiitic suites [*Miyashiro*, 1974], as do whole rock compositions for most volcanic centers from the Lesser Antilles arc [*Smith and Roobol*, 1990, p. 74]. In detail, the FeO*/MgO data reflect differences in the experimental f_{O_2}: data from the moderately oxidizing and highly oxidizing experiments plot on/above and below, respectively, the reference line (Figure 7). The scatter of the 876°C data points can be partly attributed to compositional modifications during quench.

4. Discussion

4.1. Phase Assemblages, Crystallization of Andesitic Magmas, and Liquid Line of Descent

The present work is in good agreement with previous phase equilibrium studies on andesites [*Eggler*, 1972; *Eggler and Burnham*, 1973; *Maksimov et al.*, 1978; *Ritchey and Eggler*, 1978; *Sekine et al.*, 1979; *Baker and Eggler*, 1987] and extends their conclusions toward higher f_{O_2}. By putting together these different studies, a general model for the crystallization of silicic andesite magmas at low pressures can be proposed.

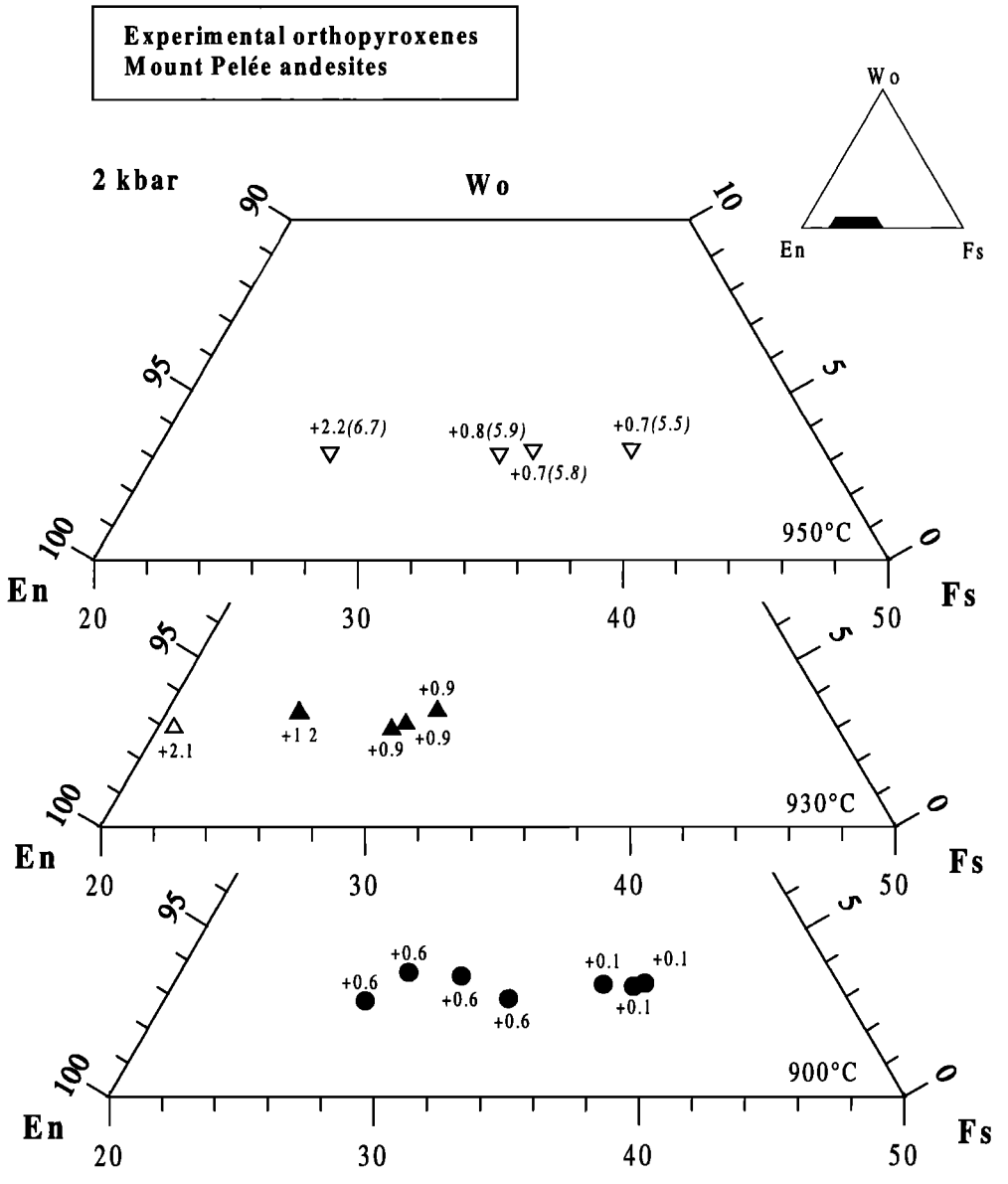

Figure 4. Composition of experimental low-Ca pyroxenes for different temperatures, f_{O_2}, and melt H_2O at 2 kbar. Solid symbols, CO_2-free conditions; open symbols: CO_2-bearing conditions. Data points (average values for a given charge) are labeled with f_{O_2} expressed as ΔNNO. Numbers in parentheses for the 950°C data points represent the melt H_2O content. Low-Ca pyroxenes become more En-rich when f_{O_2} is increased at a given temperature and melt H_2O content and when melt H_2O content is increased at a given temperature and f_{O_2}. Analytical errors are 2%.

1. Plagioclase, orthopyroxene, clinopyroxene, amphibole, and Fe-Ti oxides are the main phases stable in andesitic magmas at crustal pressures (<10 kbar). Olivine (not encountered in this study) can be present on the liquidus but quickly disappears by reaction as temperature is lowered [*Eggler*, 1972; *Grove et al.*, 1997]. Therefore olivine is not a stable phase in relatively cool (<950°C) and wet (H_2O melt > 5 wt %) silicic andesite magmas. Quartz saturation in andesite bulk compositions requires temperatures below 850°C according to our 2 kbar experimental results (Table 2) and most probably around 800°C [*Scaillet and Evans*, 1999].

2. In silicic andesite bulk compositions and for f_{O_2} between FMQ and approximately NNO + 1.5, plagioclase is the liquidus phase at 1 atm total pressure [*Eggler and Burnham*, 1973; *Ritchey and Eggler*, 1978; *Sekine et al.*, 1979]. Upon increasing pressure in this f_{O_2} range and for conditions close to H_2O saturation, plagioclase is either replaced or joined on the liquidus by either orthopyroxene [e.g., *Eggler*, 1972; *Sekine et al.*, 1979], clinopyroxene [*Maksimov et al.*, 1978; *Sekine et al.*, 1979], or magnetite (this study, Figure 3), depending on bulk composition and f_{O_2}. For f_{O_2} progressively increasing above approximately NNO + 1.5, the replacement of plagioclase by magnetite on the liquidus is expected to occur at progressively lower pressures. At sufficiently high pressures (close to CO_2-free conditions), amphibole becomes either the liquidus or a near liquidus phase for all compositions studied [*Eggler*, 1972; *Eggler and Burnham*, 1973; *Maksimov et al.*, 1978, this study, Figure 3].

3. Modal data (this study) show that plagioclase is by far the most abundant crystalline phase at 2-3 kbar, being followed by

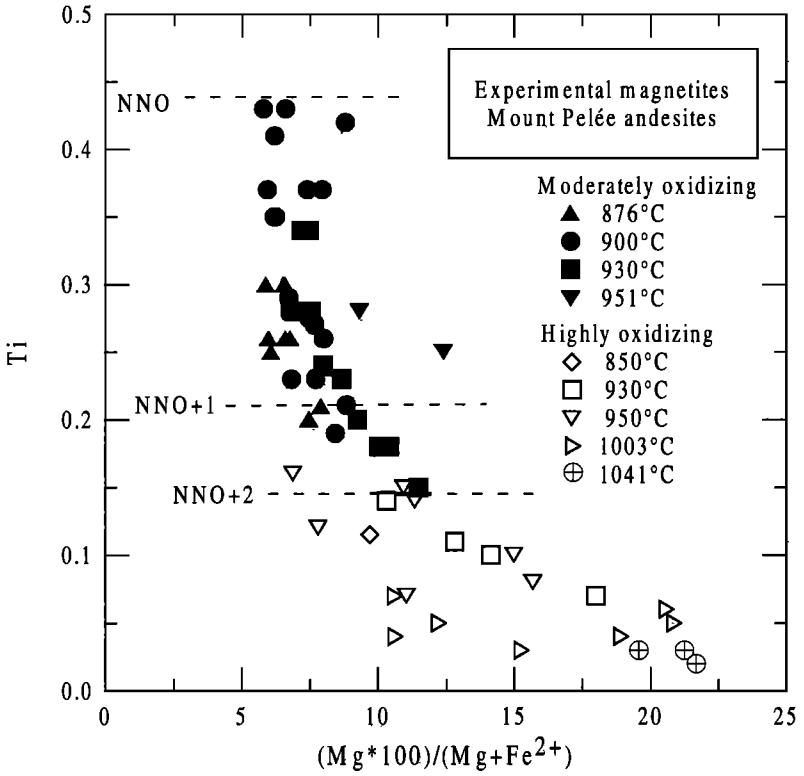

Figure 5. Composition of experimental magnetites for different temperatures and f_{O_2} at 2 kbar. Magnetite structural formulae calculated using the procedure of *Andersen et al.* [1993]. Data points (average values for a given charge) include both CO_2-free and -bearing charges and different phase assemblages. Analytical errors are 2%.

orthopyroxene and magnetite in decreasing order of abundance. Even for the most oxidizing experiments, modal proportions of magnetite never exceed 5 wt % (Table 2), which places a limit on the extent of Fe depletion that can be achieved by magnetite fractionation. In this pressure range (presumably also at lower pressures and at higher pressures if the melt is too H_2O-poor for amphibole to crystallize), pl + opx + mt fractionation essentially controls liquid compositions in silicic andesite magmas. In this study, clinopyroxene, amphibole, and ilmenite were rarely found to be present in proportions higher than a few weight percent, and there is no indication that the major mineral and melt compositions are significantly affected by the presence of these minor phases (compare, for example, compositions of the D29/2 and P1D/1 charges, Table 3). Our data demonstrate that liquids at equilibrium with pl + opx + mt evolve continuously from andesitic to rhyolitic with progressive crystallization. At 900°C, ~40% crystallization (in wt %) is required to generate a liquid composition with about 70 wt % SiO_2 (anhydrous basis) from a silicic andesite magma (Tables 2 and 3). In contrast, at higher pressures (above 3.5 kbar in this study, Figure 3) and for H_2O-rich conditions, amphibole crystallizes in elevated proportions on the liquidus (Table 2), and, therefore, am + mt fractionation controls liquid compositions during crystallization. Fractionating assemblages in silicic andesite magmas might therefore strongly change with pressure, provided that melt H_2O contents are high enough to stabilize amphibole. Since it is likely that liquids at equilibrium with am + mt will differ from those at equilibrium with pl + opx + mt, it can be expected that pressure will also influence significantly the major and trace element compositions of residual liquids.

4. An isobaric reduction of the melt H_2O content causes saturation temperatures for plagioclase, the two pyroxenes, and Fe-Ti oxides to increase. For a reduction of the first 2 wt % H_2O at 2 kbar, saturation temperatures increase by about 50°C (Figure 2), the same as in previous studies [*Eggler*, 1972; *Eggler and Burnham*, 1973], and are relatively uniform whatever the phase considered. In contrast, amphibole saturation curves show some disagreement. According to *Eggler and Burnham* [1973], amphibole saturation is almost independent of the melt H_2O content between 4.5 and 9.5 wt % H_2O. Our results show a positive dependence of amphibole saturation temperature with melt H_2O content, both at 2 and 4 kbar and for the two f_{O_2} ranges investigated. Such contrasted results might be caused by different experimental procedures and conditions. *Eggler and Burnham* [1973] used a crystal-bearing lava as starting material, and their melting experiments were of shorter durations than ours. They studied the dependence of amphibole stability with the melt H_2O content at 5 kbar and above, i.e., at higher pressures than in this study. Alternatively, amphibole stability is influenced by compositional factors: the two andesite compositions used by *Eggler* [1972] and *Eggler and Burnham* [1973] are more Na_2O- and MgO-rich than those from this study.

4.2. Fe-Ti Oxides, Amphibole, and Pyroxene in Andesitic Magmas: The Role of f_{O_2}

Earlier studies on silicic andesite bulk compositions were all carried out under relatively reducing conditions (FMQ $\leq f_{O_2} \leq$ NNO). Results from these studies are typically characterized by (1) the common presence of two Fe-Ti oxide phases (ilmenite and magnetite) and (2) the late appearance of Fe-Ti

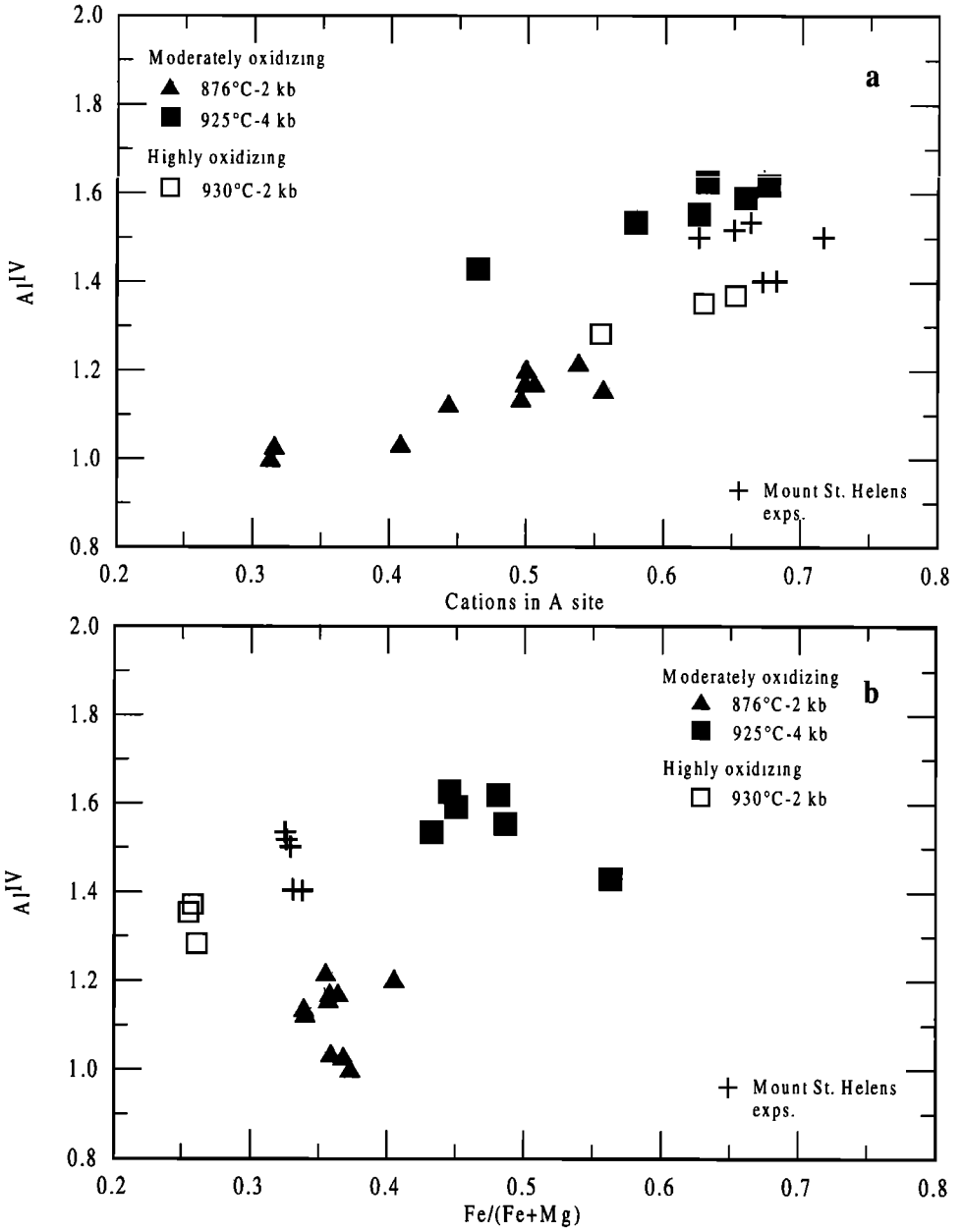

Figure 6. Compositions of experimental amphiboles (individual analyses). (a) Tetrahedral aluminium (Al^{IV}) versus number of cations in the A site; (b) Al^{IV} versus Fe / (Fe + Mg), with total Fe as FeO. Amphibole compositions from the Mount St. Helens experiments at 2.0-2.2 kbar, 875-922°C, and f_{O_2} between GCH (graphite + methane) and NNO+1.2 taken from *Rutherford et al.* [1985] and *Rutherford and Devine* [1988]. Amphibole structural formulae calculated on a 23 O basis using the procedure of *Richard and Clarke* [1990]. Analytical errors are 2%.

oxides in the crystallization sequence [*Eggler*, 1972; *Eggler and Burnham*, 1973]. Data from those studies, in particular concerning the stability of Fe-Ti oxides, have been influential in the development of objections against fractional crystallization for the origin of andesites [e.g., *Eggler*, 1972; *Eggler and Burnham*, 1973]. Subsequently, it was pointed out by several authors that additional experiments above FMQ could well lead to magnetite crystallization closer to the liquidus [e.g., *Arculus and Wills*, 1980; *Gill*, 1981]. *Sekine et al.* [1979] found no magnetite in experiments performed at NNO on andesites but estimated that f_{O_2} conditions about 1 log unit above the NNO buffer might have been sufficient to cause precipitation of titanomagnetite on the liquidus.

The influence of f_{O_2} has been systematically studied between approximately NNO and NNO + 3 in this study and found to be more important than previously considered. Changes in f_{O_2} affect not only the stability of Fe-Ti oxides [*Rutherford et al.*, 1985; *Rutherford and Devine*, 1988] but also that of amphibole and pyroxenes. Variations in compositions of ferromagnesian phases are correlated with the evolution of their respective stability fields with changing f_{O_2}.

4.2.1. Fe-Ti oxides. At ~2 kbar and 900°C, both ilmenite and magnetite crystallized when f_{O_2} was $\leq$ NNO, whereas magnetite is the sole Fe-Ti oxide phase from ΔNNO = + 0.4 to + 0.6. Ilmenite also coexists with magnetite in some charges at 3.1 and 4.2 kbar under conditions slightly more oxidizing than

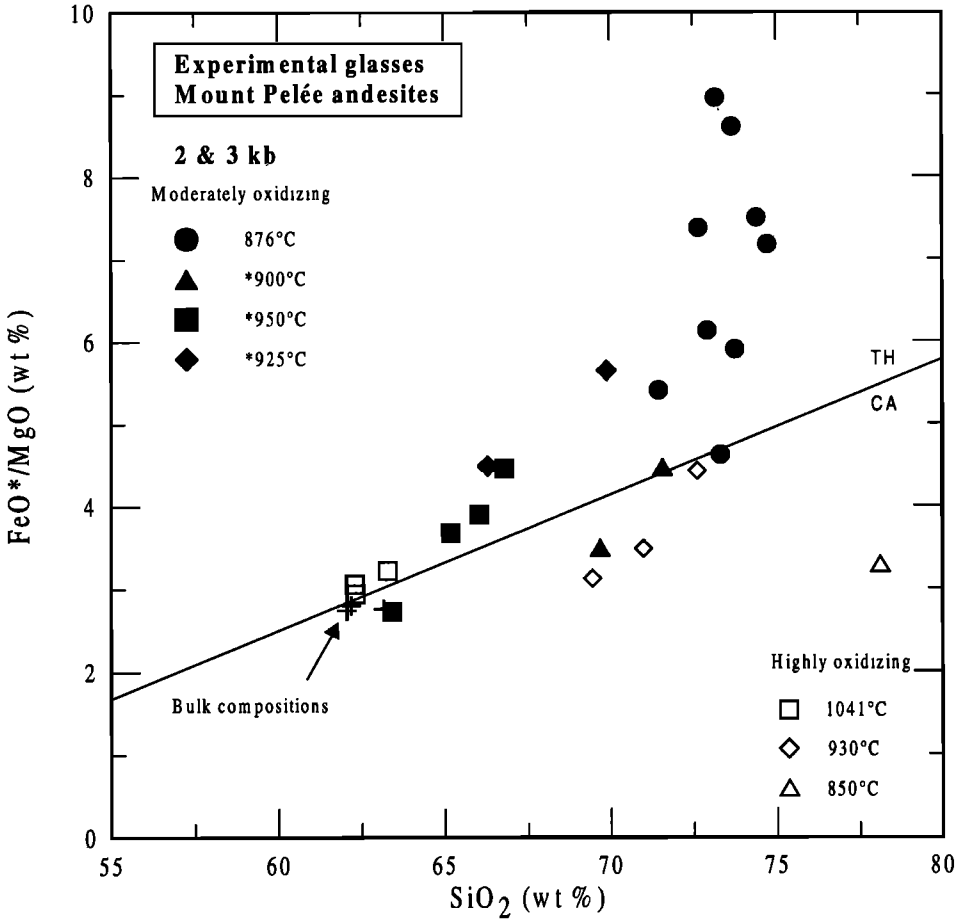

Figure 7. Plot of FeO*/MgO versus SiO_2 for the 2 and 3 kbar experimental glasses. Data (average values for a given charge) are from Tables 1 and 3 and *Martel* [1996]. See Table 2 for experimental conditions. Data points from the rapid-quench experiments labeled with asterisks. The reference boundary between calk-alkaline and tholeiitic suites is from *Miyashiro* [1974]. Analytical errors are 2%.

NNO (Table 2). This suggests that at ~900°C, the coexistence of magnetite and ilmenite in andesitic magmas requires $f_{O_2} \leq$ approximately NNO, consistent with the data of *Eggler and Burnham* [1973]. Above ΔNNO = +0.4, the thermal stability of magnetite is strongly f_{O2}-dependent. At 2 kbar, magnetite and plagioclase are the liquidus phases between NNO and NNO + 1, and magnetite alone is on the liquidus in the range NNO + 2 to NNO + 3, crystallizing from temperatures above 1040°C (Figure 3). This stresses the sensitivity of magnetite stability on f_{O2} conditions above NNO and demonstrates that for f_{O2} conditions typical of calk-alkaline magmatism (~NNO + 1 [*Gill*, 1981]), magnetite will be either a liquidus or a near-liquidus phase for silicic andesite compositions. However, the 1 atm experimental data [*Eggler and Burnham*, 1973; *Ritchey and Eggler*, 1978; *Sekine et al.*, 1979] show that even under strongly oxidizing conditions (ΔNNO ~ 3), plagioclase assumes the liquidus for either H_2O-poor or dry conditions. Therefore, for magnetite to be a liquidus/near-liquidus phase in silicic andesite magmas, both relatively high f_{O_2} and H_2O-rich conditions are needed.

Compositions of magnetite show important variations with f_{O_2} and temperature (Figure 5). Magnetites crystallizing in the moderately oxidizing experiments have lower $(Mg*100)/(Mg+Fe^{2+})$ and higher Ti than those from the highly oxidizing experiments. Therefore magnetite composition alone is a sensitive indicator of f_{O_2} in andesite magmas.

4.2.2. Amphibole. Previous studies have recognized the strong influence of pressure and H_2O melt on amphibole stability in andesitic magmas [*Eggler*, 1972; *Eggler and Burnham*, 1973; *Maksimov et al.*, 1978]. The possibility that f_{O_2} also has some influence on amphibole stability has been investigated more recently. *Rutherford and Devine* [1988] extended the experiments of *Rutherford et al.* [1985] on the Mount St. Helens dacites toward higher f_{O_2}, between the NNO and MNO buffers. The thermal stability of amphibole was not significantly dependent on f_{O_2} between FMQ and approximately NNO + 1.5. Amphiboles in this f_{O_2} range were found to have compositions very close to each other (Figure 6). Above NNO + 1.5, *Rutherford and Devine* [1988] obtained more magnesian amphiboles (Fe/(Fe+Mg) = 0.15), but their maximum thermal stability was not determined systematically. Our study shows that increasing f_{O_2} above NNO + 1 promotes amphibole stability. At 2 kbar under CO_2-free conditions the maximum thermal stability of amphibole increases by 60°C when f_{O_2} is raised from NNO/NNO + 1 to NNO + 2/NNO + 3 (Figure 3). This effect is accompanied by marked changes in amphibole composition. Amphiboles stable under wet,

strongly oxidized (greater than NNO + 2) conditions are Mg-rich (Figure 6). Crystallization of more refractory amphibole compositions under strongly oxydizing conditions is consistent with their enhanced thermal stability. In comparison with amphiboles crystallizing under moderately oxidizing conditions, lower pressures would be needed for these Mg-rich amphiboles to become liquidus phases under near CO_2-free conditions.

4.2.3. Pyroxenes. Except for experiments at near CO_2-free conditions, increasing f_{O_2} from NNO/NNO + 1 to NNO + 2/NNO + 3 does not significantly affect low-Ca pyroxene stability (Figure 2). However, differences exist between studies. In the Paricutin andesite, low-Ca pyroxene is the liquidus phase for melt H_2O contents ranging from saturation to a_{H_2O} ~ 0.2 at 5 kbar [*Eggler*, 1972]. In the Mount Hood andesite, low-Ca pyroxene is a near-liquidus phase, being second in the sequence after plagioclase [*Eggler and Burnham*, 1973]. In contrast, low-Ca pyroxene in this study appears relatively late. It follows plagioclase and magnetite at 2 kbar in both series of experiments and amphibole, magnetite, and plagioclase at 4 kbar for moderately oxidizing conditions. The contrasted behavior of low-Ca pyroxene between these studies probably reflects differences in bulk composition. There is a negative correlation between low-Ca pyroxene saturation temperature and the FeO*/MgO of the starting andesite. Compositions from Mount Pelée have FeO*/MgO of 2.7-2.8 (Table 1), significantly higher than the Mount Hood andesite (2.1 [*Eggler and Burnham*, 1973]) and nearly twice the value for the Paricutin andesite (1.4 [*Eggler*, 1972]). Low-Ca pyroxene stability is enhanced in magnesian andesites probably because En-rich compositions are stabilized.

At near CO_2-free conditions, f_{O_2} strongly affects the stability of low-Ca pyroxene (Figure 2). Increasing f_{O_2} from NNO/NNO + 1 to NNO + 2/NNO + 3 decreases the low-Ca pyroxene saturation temperature by ~40°C (if extrapolated to CO_2-free conditions). The ferromagnesian silicate phase assemblage in the CO_2-free 930°C highly oxidizing charge P1R/12 consists of high-Ca pyroxene + amphibole instead of low-Ca pyroxene, suggesting a reaction relation between low-Ca pyroxene and high-Ca pyroxene + amphibole. Similar reaction relationships between low-Ca pyroxene and amphibole have been found previously in intermediate to silicic compositions [*Naney*, 1983; *Scaillet and Evans*, 1999]. Resorption of orthopyroxene and crystallization of amphibole is usually attributed to an increase of melt H_2O content during crystallization [*Naney*, 1983]. Our data show that under near CO_2-free conditions the reaction is promoted by an increase of f_{O_2}. This effect could result from the preferential stabilization of Fe^{3+}-bearing assemblages (i.e., am + cpx) upon increasing f_{O_2} and melt Fe^{3+}/Fe^{2+}.

By comparison to low-Ca pyroxene, the high-Ca pyroxene saturation temperature slightly shifts toward higher temperatures (~20-40°C) under highly oxidizing conditions. Note, however, that high-Ca pyroxene saturation curves in this study are approximate because augites are present sporadically in the run products. Nevertheless, high-Ca pyroxenes from the CO_2-free highly oxidizing 930°C charge (P1R/12, Table 2) have compositions differing from those crystallizing under moderately oxidizing conditions, the compositional changes (i.e., higher En and Wo) being consistent with their enhanced thermal stability. The only experimental study involving andesites that documented the occurrence of high-Ca pyroxene on the liquidus above 3 kbar CO_2-free is that of *Maksimov et al.* [1978], performed on an andesite having 7.6 wt % CaO (6.1-6.2 in this study, 6.3 for the Paricutin andesite), suggesting that elevated CaO contents favor crystallization of high-Ca rather than low-Ca pyroxene for equivalent MgO contents.

5. Concluding Remarks

The present work extends the experimental database for silicic andesite magmas toward higher f_{O_2} (greater than NNO), compatible with conditions typical of calk-alkaline magmatism. The main result is the demonstration of an important influence of f_{O_2} on phase assemblages and compositions crystallizing from silicic andesites below 5 kbar. In particular, magnetite is a liquidus or a near-liquidus phase in hydrous silicic andesite magmas for f_{O_2} conditions more oxidizing than NNO + 1. Magnetite compositions (Ti and Mg #) are strongly dependent on f_{O_2} above NNO and constitute a sensitive indicator of f_{O_2} in andesite magmas. Magnetite fractionation exerts control of the FeO*/MgO of the residual liquids. At ~900°C the coexistence of magnetite and ilmenite in silicic andesite magmas requires $f_{O_2} \leq$ NNO. Redox conditions also play an important role on the stability of amphibole and low-Ca and high-Ca pyroxenes, in addition to bulk magma composition. Compositions of these ferromagnesian phases are systematically correlated with changing f_{O_2} conditions. The demonstration that magnetite can be a liquidus phase for $f_{O_2} \geq$ NNO + 1 should stimulate reexamination for the mechanisms of generation of andesites by fractionation from hydrous and oxidized basaltic parents.

Acknowledgments. This paper forms part of the Ph.D. thesis of C. Martel and has benefited from discussions with Malcolm Rutherford. We acknowledge John Eichelberger, Jim Luhr, and James Gardner for reviews. This study was supported by PNRN.

References

Albarède, F., *Introduction to Geochemical Modelling*, Cambridge Univ. Press, New York, 1995.

Andersen, D.J., D. H. Lindsley, and P. M. Davidson, QUILF: A Pascal program to assess equilibria among Fe-Mg Ti oxides, pyroxenes, olivine, and quartz, *Comput. Geosci., 19*, 1333-1350, 1993.

Arculus, R. J., and K. J. A. Wills, The petrology of plutonic blocks and inclusions from the Lesser Antilles, *J. Petrol., 21*, 743-799, 1980.

Bacon, C. R., and M. M. Hirschmann, Mg/Mn partitioning as a test for equilibrium between coexisting Fe-Ti oxides, *Am. Mineral., 73*, 57-61, 1988.

Baker, D. R., and D. H. Eggler, Compositions of anhydrous and hydrous melts coexisting with plagioclase, augite, and olivine or low-Ca pyroxene from 1 atm to 8 kbar: Applications to the Aleutian volcanic center of Atka, *Am. Mineral., 72*, 12-28, 1987.

Behrens, H., C. Romano, M. Nowak, F. Holtz, and D. B. Dingwell, Near-infrared determination of water species in glasses of the system $MAlSi_3O_8$ (M = Li, Na, K): an interlaboratory study, *Chem. Geol., 128*, 41-63, 1996.

Burnham, C. W., The importance of volatile constituents, in *The Evolution of Igneous Rocks*, edited by H.S. Yoder, pp. 439-482, Princeton Univ. Press, Princeton, N.J., 1979.

Chou, I. M., Oxygen buffer and hydrogen sensor technique at elevated pressures and temperature, in *Hydrothermal Experimental Techniques*, edited by H. L. Barnes and G. C. Ulmer, pp. 61-99, John Wiley, New York, 1987.

Defant, M. J., and M. S. Drummond, Derivation of some modern arc magmas by melting of young subducted lithosphere, *Nature*, *347*, 662-665, 1990.

Devine, J. D., J. E. Gardner, H. P. Brack, G. D. Layne, and M. J. Rutherford, Comparison of microanalytical methods for estimating H_2O contents of silicic volcanic glasses, *Am. Mineral.*, *80*, 319-328, 1995.

Eggler, D. H., Water-saturated and undersaturated melting relations in a Paricutin andesite and an estimate of water content in the natural magma, *Contrib. Mineral. Petrol.*, *34*, 261-271, 1972.

Eggler, D. H., and C. W. Burnham, Crystallization and fractionation trends in the system andesite-H_2O-CO_2-O_2 at pressures to 10 kb, *Geol. Soc. Am. Bull.*, *84*, 2517-2532, 1973.

Eichelberger, J.C., Origin of andesite and dacite: evidence of mixing at Glass Mountain in California and at other Circum-Pacific volcanoes, *Geol. Soc. Am. Bull.*, *86*, 1381-1391, 1975.

Fenn, P. M., The nucleation and growth of alkali feldspars from hydrous melts, *Can. Mineral.*, *15*, 135-161, 1977.

Fichaut, M., R. C. Maury, H. Traineau, D. Westercamp, J.-L. Joron, A. Gourgaud, and C. Coulon, Magmatology of Mount Pelée (Martinique, F.W.I), III, Fractional crystallisation versus magma mixing, *J. Volcanol. Geotherm. Res.*, 38, 189-213, 1989.

Gaetani, G. A., T. L. Grove, and W. B. Bryan, The influence of water on the petrogenesis of subduction-related igneous rocks, *Nature*, *365*, 332-334, 1993.

Ghiorso, M. S., and R. O. Sack, Fe-Ti oxide geothermometry: thermodynamic formulation and estimation of intensive variables in silicic magmas, *Contrib. Mineral. Petrol.*, *108*, 485-510, 1991.

Gill, J. B., *Orogenic Andesites and Plate Tectonics*, Springer-Verlag, New York, 1981.

Green, D. H., Experimental testing of "equilibrium" partial melting of peridotite under water-saturated, high pressure conditions, *Can. Mineral.*, *14*, 255-268, 1976.

Green, T. H., and A. E. Ringwood, Genesis of the calc-alkaline igneous rock suite, *Contrib. Mineral. Petrol.*, *18*, 105-162, 1968.

Grove, T. L., J. M. Donnelly-Nolan, and T. Housh, Magmatic processes that generated the rhyolite of Glass Mountain, Medecine Lake volcano, N. California, *Contrib. Mineral. Petrol.*, *127*, 205-223, 1997.

Helz, R. T., Phase relations of basalts in their melting range at P_{H2O} = 5 kb as a function of oxygen fugacity, I, Mafic phases, *J. Petrol.*, *14*, 249-302, 1973.

Helz, R. T., Phase relations of basalts in their melting range at P_{H2O} = 5 kb as a function of oxygen fugacity, II, Melt composition, *J. Petrol.*, *17*, 139-193, 1976.

Holtz, F., M. Pichavant, P. Barbey, and W. Johannes, Effects of H_2O on liquidus phase relations in the haplogranite system at 2 and 5 kbar, *Am. Mineral.*, *77*, 1223-1241, 1992.

Kay, R. W., Aleutian magnesian andesites: melts from subducted Pacific Ocean crust, *J. Volcanol. Geotherm. Res.*, *4*, 117-132, 1978.

Kushiro, I., N. Shimizu, Y. Nakamura, and S. Akimoto, Compositions of co-existing liquids and solid phases formed upon melting of natural garnet and spinel lherzolites at high pressures: A preliminary report, *Earth Planet. Sci. Lett.*, *14*, 19-25, 1972.

Maksimov, A. P., A. A. Kadik, E. Y. Korovushkina, and B. V. Ivanov, Crystallization of an andesite melt with a fixed water content at pressures up to 12 kbar, *Geochem. Int.*, *15*, 20-29, 1978.

Martel, C., Conditions pré-éruptive et dégazage des magmas andésitique de la Montagne Pelée (Martinique): Etude pétrologique et expérimentale, Ph.D. thesis, Univ. of Orléans, Orléans, France, 1996.

Merzbacher, C., and D. H. Eggler, A magmatic geohygrometer: Application to Mount St. Helens and other dacitic magmas, *Geology*, *12*, 587-590, 1984.

Miyashiro, A., Volcanic rock series in island arcs and active continental margins, *Am. J. Sci.*, *283*, 993-1033, 1974.

Mysen, B. O., I. Kushiro, I. A. Nicholls, and A. E. Ringwood, A possible mantle origin for andesitic magmas: Discussion of a paper by Nicholls and Ringwood, *Earth Planet. Sci. Lett.*, *21*, 221-229, 1974.

Naney, M.T., Phase equilibria of rock-forming ferromagnesian silicates in granitic systems, *Am. J. Sci.*, *283*, 993-1033, 1983.

Nicholls, I. A., and A. E. Ringwood, Effect of water on olivine stability in tholeiites and the production of silica saturated magmas in the island arc environment, *J. Geol.*, *81*, 285-300, 1973.

Pichavant, M., The effects of boron and water on liquidus phase relations in the haplogranite system at 1 kbar, *Am. Mineral.*, *72*, 1056-1070, 1987.

Richard, L.R., and Clarke D.B., Amphibol: A program for calculating structural formulae and for classifying and plotting chemical analyses of amphiboles, *Am. Mineral.*, 75, 421-423, 1990.

Ritchey, J. L., and D. H. Eggler, Amphibole stability in a differentiated calc-alkaline magma chamber: An experimental investigation, *Year Book Carnegie Inst. Washington 1977-1978*, 790-793, 1978.

Roux, J., and A. Lefevre, A fast quench device for IHPV, *Eur. J. Mineral.*, *4*, 279-281, 1992.

Roux, J., F. Holtz, A. Lefèvre, and F. Schulze, A reliable high temperature setup for internally heated pressure vessel: Applications to silicate melt studies, *Am. Mineral.*, *79*, 1145-1149, 1994.

Rutherford, M.J., and J. D. Devine, The May 18, 1980, eruption of Mount St. Helens, 3, Stability and chemistry of amphibole in the magma chamber, *J. Geophys. Res.*, *93*, 11,949-11,959, 1988.

Rutherford, M.J., H. Sigurdsson, S. Carey, and A. Davis, The May 18, 1980, eruption of Mount St. Helens, 1, Melt composition and experimental phase equilibria, *J. Geophys. Res.*, *90*, 2929-2947, 1985.

Scaillet, B., and B. W. Evans, The June 15, 1991 eruption of Mount Pinatubo, I, Phase equilibria and pre-eruption *P-T-*f_{O2}-f_{H2O} conditions of the dacite magma, *J. Petrol.*, *40*, 381-411, 1999.

Scaillet, B., M. Pichavant, J. Roux, G. Humbert, and A. Lefèvre, Improvements of the Shaw membrane technique for measurement and control of f_{H2} at high temperatures and pressure, *Am. Mineral.*, *77*, 647-655, 1992.

Scaillet, B., M. Pichavant, and J. Roux, Experimental crystallization of leucogranite magmas, *J. Petrol.*, *36*, 663-705, 1995.

Sekine, T., T. Katsura, and S. Aramaki, Water saturated phase relations of some andesites with application to the estimation of the initial temperature and water pressure at the time of eruption, *Geochim. Cosmochim. Acta*, *43*, 1367-1376, 1979.

Sisson, T. W., and T. L. Grove, Experimental investigations of the role of H_2O in calc-alkaline differentiation and subduction zone magmatism, *Contrib. Mineral. Petrol.*, *113*, 143-166, 1993a.

Sisson, T. W., and T. L. Grove, Temperatures and H_2O contents of low-MgO high alumina basalts, *Contrib. Mineral. Petrol.*, *113*, 167-184, 1993b.

Smith, A. L., and M. J. Roobol, Mount Pelée, Martinique, A study of an active island-arc volcano, *Mem. Geol. Soc. Am.*, *175*, 1990.

Stern, R. J., On the origin of andesite in the northern Mariana island arc: Implications from Agrigan, *Contrib. Mineral. Petrol.*, *68*, 207-219, 1979.

Taylor, J. R., V. J. Wall, and M. I. Pownceby, The calibration and application of accurate redox sensors, *Am. Mineral.*, *77*, 284-295, 1992.

Yogodzinski, G. M., O. N. Volynets, A. V. Koloskov, N. I. Seliverstov, and V. V. Matvenkov, Magnesian andesites and the subduction component in a strongly calc-alkaline series at Piip volcano, far western Aleutian, *J. Petrol.*, *35*, 163-204, 1994.

J.-L. Bourdier, Département des Sciences de la Terre, Université d'Orléans, BP 6759, F-45067 Orléans cedex, France. (jean-louis.bourdier@univ-orleans.fr)

F. Holtz, M. Pichavant, and B. Scaillet, Centre de Recherches sur la Synthèse et chimie des Minéraux, CNRS, 1A rue de la Férollerie, F-45071 Orléans, France. (caroline.martel@uni-bayreuth.de)

C. Martel, Bayerisches Geoinstitut, Universität Bayreuth, D-95440 Bayreuth, Germany. (caroline.martel@uni-bayreuth.de)

H. Traineau, BRGM, Service Géologique National, F-45060 Orléans cedex, France.

(Received July 15, 1998; revised May 17, 1999; accepted May 27, 1999.)